PEOPLE'S DEMOCRATIC REPUBLIC OF ALGERIA

MINISTRY OF HIGHER EDUCATION AND SCIENTIFIC RESEARCH

Mohamed El-Bachir El-Ibrahimi University - Bordj Bou Arreridj

Faculty of Science and Technology

Department of Electronics

Memoire

Presented for obtaining

THE MASTER'S DIPLOMA

FILIERE: Telecommunication

Specialty: Telecommunications System

By

TABABOUCHET Hamouda

BOUBETRA Lotfi

Entitled

Analytical Evaluation of Congruence Code-Based Time-Hopping Slot Index Table Generation in Pseudolite Positioning Systems.

Supported on: 12/07/2024

Before the jury composed of:

Name	*Grade*	*Quality*	*Establishment*
M. Salah.Edine.MEZAACHE	MCB	President	Univ-BBA
M. Wafa.FENINICHE	MAB	Examiner	Univ-BBA
M. Mustapha FLISSI	MCA	Supervisor	Univ-BBA
M. Ayoub BENGHERABI	PhD Student	Co-Supervisor	Univ-BBA

College year 2023/2024

Acknowledgements

First and foremost, we express our profound gratitude to Almighty God for granting us the courage and determination to complete this project. We extend heartfelt thanks to our parents and beloved families for their unwavering support and encouragement over the years. Our deep appreciation goes to our supervisor, Mr. ***Mustapha Felissi****, for his belief in us, continuous support, and guidance throughout our work.*

We are equally grateful to Mr. ***Ayoub Bengherabi****, our assistant supervisor, for his steadfast support and significant contributions to our success, never leaving our side during this journey. We also wish to thank our fellow student,* ***SEGUENI Oussama****, whose creative input in the design and structure of our memo was invaluable, and who supported us throughout the process. Lastly, we extend our sincere thanks to the jury members for honoring us by evaluating our work. We aspire to meet their expectations. Our gratitude also goes to all our friends and colleagues, especially those who provided us with moral support.*

Dedication

I dedicate this humble work:

To the memory of my father, may he rest in peace

To my dear mum, who has always been there for me and supported me

TABABOUCHET Hamouda

. *Dedication*

I dedicate this dissertation to:

My dear ***parents****, who have always been by my side and supported me throughout my long years of study. As a token of my gratitude, may they find here the expression of my deepest gratitude for all their efforts and means to see me succeed in my studies.*

To my dear brothers ***Chaouki*** *and* ***Youcef****.*

To my dear ***Sisters****.*

To my partner ***Hamouda****.*

To all my loved ones.

To all my friend.

BOUBETRA LOTFI

Table of Contents

Chapter 2 : Time Hopping Pseudolite's SIT generation

Chapter 3 : Result and Discussion

List of Figures

List of Tables

List of Equations

Acronyms and Abbreviations

ACF	Autocorrelation function
AWGN	Additive white Gaussian noise
BPSK	Binary Phased Shift Keying
CC	Congruence Codes
C/A	Coarse/Acquisition
CCF	Cross-correlation function
CDMA	Code Division Multiple Access
DLL	Delay Locked Loop
DOD	Department of Defense
DSSS	Direct Sequence Spread Spectrum
FFT	Fast Fourier Transform
GNSS	Global Navigation Satellite System
GPS	Global Positioning System
IFFT	Inverse Fast Fourier Transform
INS	Inertial Navigation Systems
NCO	Numerically Controlled Oscillator
PL	Pseudolite
PLPS	Pseudolite Positioning Systems
PLL	Phase Locked Loop
PRN	Pseudo Random Noise
PSD	Power Spectral Density
PPS	Precise Position Service
RP	Rand Perm
SIC	Successive Interference Cancellation
SIR	Signal-to-Interference Ratio
SIT	Slot Index Table
SNR	Signal-to-Noise Ratio
SPS	Standard Position Service
TDMA	Time Division Multiple Access
TH	Time Hopping
THSI	Time Hopping Slot Index

Abstract

This Master's Thesis examines the Time-Hopping Slot Index Table (SIT) generation method using congruence codes (CC) within Pseudolite Positioning Systems (PLPS), a recent and reliable enhancement to traditional Global Navigation Satellite Systems (GNSS). The study will analyze correlation characteristics, Power Spectral Density (PSD) property and the histogram distribution of time-hopping intervals, following the established methodology. We aim to assess the effectiveness of this method in pulse position detection, comparing it with alternative approaches under various Signal-to-Noise Ratio (SNR) conditions. The simulations shows that compared with other similar scheme, the SITs given by the CC-based method can obtain better correlation performance and detection performance in the receiver,

Keywords: Time-Hopping, Slot Index Table, Pseudolite Positioning Systems, GNSS, Congruence Codes.

ملخص

تبحث رسالة الماستر هذه في طريقة توليد جدول مؤشر فواصل القفز الزمني (SIT) باستخدام رموز التطابق في أنظمة تحديد المواقع الكاذبة(PLPS) ، وهو تحسين حديث وموثوق به للنظم العالمية التقليدية لسواتل الملاحة العالمية .(GNSS) وستقوم الدراسة بتحليل خصائص الارتباط وملاءمة الكثافة الطيفية للقدرة والتوزيع التكراري لفترات التنقل الزمني، باتباع المنهجية المتبعة. ونحن نهدف إلى تقييم فعالية هذه الطريقة في الكشف عن موقع النبضات، ومقارنتها مع الأساليب البديلة في ظل ظروف مختلفة لنسبة الإشارة إلى الضوضاء .(SNR) تُظهر المحاكاة أنه بالمقارنة مع المخططات الأخرى المماثلة، يمكن أن تحصل SITs التي تقدمها الطريقة القائمة على CC على أداء ارتباط وأداء كشف أفضل في جهاز الاستقبال.

الكلمات المفتاحية: التنقل بين الأزمنة، جدول مؤشر الفتحة، أنظمة تحديد المواقع الزائفة، النظم العالمية لسواتل الملاحة، رموز التطابق.

Résumé

Ce mémoire de master examine la méthode de génération du tableau d'indexation des créneaux (SIT) de saut temporel utilisant des codes de congruence dans les systèmes de positionnement pseudolites (PLPS), une amélioration récente et fiable des systèmes traditionnels de navigation globale par satellite (GNSS). L'étude analysera les caractéristiques de corrélation et la propreté de la densité spectrale de puissance ,la distribution de l'histogramme des intervalles de saut temporel, en suivant la méthodologie établie. Nous visons à évaluer l'efficacité de cette méthode dans la détection de la position des impulsions, en la comparant à d'autres approches dans différentes conditions de rapport signal/bruit (SNR). Les simulations montrent que, par rapport à d'autres systèmes similaires, les SIT obtenus par la méthode basée sur le CC permettent d'obtenir de meilleures performances en matière de corrélation et de détection dans le récepteur .

Mots-clés : Saut temporel, table d'index des créneaux, systèmes de positionnement pseudolites, GNSS, codes de congruence.

General Introduction

General Introduction

In GNSS-denied environments, the PL is a ground-based transmitter to improve GNSS availability and integrity or establish a standalone local positioning system. Yet, its use in such settings can lead to significant interference, known as "near-far" interference, with weak GNSS or other PL signals at the receiver [1] [2] [3]. To mitigate this interference, different techniques have been suggested, with the TH pulsed PL signal emerging as a promising solution. [1][2][4]

The TH-pulsed PL signal is formed by gating a continuous local-generated GNSS-like signal with a sequence of TH pulses controlled by a SIT. Effective SIT design involves maintaining pseudo-random THSIs to preserve the spectral shape, aligning spreading factors, and assigning unique SITs to each PL for signal distinction .[2] [3]

According to the search results, a new block-based [1] approach for generating the SIT for TH pulsed PL signals is introduced. The method involves creating different THSI base matrices using constructed congruence codes, combining these matrices, and then selecting specific rows to form a new matrix representing the SIT for a particular PL. Different SITs can be generated for each PL by modifying the combined matrices. This proposed technique provides improved SIT correlation and detection performance compared to existing schemes while still meeting the spreading factor requirements of the PL signal. [2] [5]

The aim of this Master's thesis in telecommunications systems is to validate this method by numerical simulation to determine its effectiveness in generating pseudo-random positions for TH pulses in the pseudolite signal.

Document organization:

The first chapter presents the GPS satellite positioning system and the pseudolite positioning system and near far problem with solution.

The second chapter presents the signal model of TH pulsed PL, and the generation methods of THSI base matrices and SITs, analyses the correlation properties of formed SITs, describes the SIT detection method of the received PL signal

The third chapter presents the result of simulations the performance of this new method of the formed SITs.

Chapter 1 :
GPS System and Pseudolite

1.1 Introduction

The Global Positioning System has been fully operational since 1994, developed by the American Department of Defense. It consists of approximately 24 satellites orbiting Earth, offering 24-hour weather-independent positioning services. Similarly, GLONASS operated by Russia features 24 satellites in three orbital planes. These Global Navigation Satellite Systems, including GPS, GLONASS, and GALILEO, transmit coherent carriers in the microwave L-band, allowing GNSS receivers to determine positions instantaneously with meter-level precision. Advanced applications of GNSS use carrier phase analysis to achieve centimeter-to-millimeter precision. [6], [7], [8], [9]

The International GNSS Service IGS facilitates GNSS utilization for scientific and societal benefits, emphasizing applications requiring stringent satellite position accuracy and clock corrections in picoseconds. [10]

In this chapter, we aim to introduce The Navigation of GPS and Satellite, as well as pseudolite Navigation and the near-far problem. In this chapter, we introduce The Navigation of GPS and Satellites, as well as pseudolite Navigation and the near-far problem.

1.2 GPS satellite positioning system

1.2.1 GPS system

Global positioning system (GPS) is a satellite-based navigational technology originally devised for military purposes. A number of informative, [11-14], has proven to be a great asset in a variety of civilian applications [15] Civilian GPS provides basic location accuracy within 10 meters, but augmentation techniques can enhance accuracy to less than 1 cm. Its widespread availability and high accuracy have revolutionized personal and commercial navigation beyond its military origins. Various entities, from battlefield weapons to space shuttles and commercial airplanes, utilize GPS for positioning and navigation. [6], [7], [16], [17], [18]

1.2.2 GPS Segment

1.2.2.1 Space segment

The GPS constellation is organized into six evenly spaced orbital planes encircling the Earth, with each plane accommodating four "slots" occupied by baseline satellites. This configuration, totaling 24 slots, is strategically designed to enable users to receive signals from a minimum of four satellites from virtually any location on the planet, ensuring accurate positioning and navigation capabilities. [19]

To ensure uninterrupted coverage, the Space Force typically operates more than the required 24 GPS satellites. This surplus allows for continued service provision during the maintenance or decommissioning of baseline satellites. By maintaining an excess number of operational satellites, the GPS guarantees reliable global positioning services, safeguarding against disruptions and enhancing user confidence in the system's performance. [19]

1.2.2.2 Control segment

The GPS control segment is a vital element comprising a worldwide network of ground facilities responsible for tracking GPS satellites, monitoring their transmissions, performing analysis, and transmitting commands and data to the satellite constellation.

Within the current OCS, key facilities include a main control station, a backup main control station, 11 command and control antennas, and 16 monitoring sites. Together, these facilities ensure the efficient management and operation of the GPS satellite system, facilitating the provision of accurate positioning and navigation services worldwide. [20], [21]

1.2.2.3 User segment

The user segment of a GPS is crucial for receiving and processing signals from GPS satellites and calculating the user's three-dimensional position and time reference. This segment includes GPS receivers, such as smartphones, navigation systems, or fleet management systems. These receivers pick up signals from at least four satellites and use a mathematical technique called trilateration to determine the position as a function of the distance and angle of each satellite. [7]

1.2.3 GPS Signal

1.2.3.1 Planning frequency

By transmitting three signals across various frequency bands which are centered about certain values, the 24 GPS satellites work. These signals are important in establishing where the receiver is, how fast it is moving, and what time it is by the method of trilateration. The GPS receivers can locate their exact position on the surface of the Earth by receiving and studying these signals because they allow for triangulation. Table 1.1 Shown the frequency bands used by GPS satellites. [22]

Table 1.1 : frequency bands used by GPS satellites

Frequency Band	Center Frequency (MHz)
L1	1575.42
L2	1227.60
L5	1176.45

1.2.3.2 The Standard Position Service

The SPS is worldwide with a frequency of around 1,575.42 MHz and can be accessed by any user having a single-frequency L1 receiver. The use of the pseudo-random sequence of +1s and -1s known as Coarse Acquisition-code (C/A code) on the L1 carrier makes it possible for civil applications using GPS to work. This function is deterministic mathematically and at 1.023 MHz has a short period of 10^{-3} seconds hence making receivers acquire and identify satellites quickly. Within this scheme, each satellite is given one code only which is different from others. C/A code was initially designed for fast acquiring P(Y) code but now it is purely used for civilian purposes thereby serving as essential component in providing standard positioning services via SPS. Besides that, it follows a formula like this: (2^n-1), where n represents an integer number. [6],[22], [23], [24] [25]

1.2.3.3 The Precise Position Service

The Precision Code, commonly called P(Y) code, is the essential military application on the L1 and the L2 military carriers because of its special construction for military purposes. Working at the frequency of f_o = 10.23 MHz, this code relies on a pseudo-random sequence as the basis for its operation.

The access to the P-Code is restricted to the authorized personnel only with the A.S. (anti-spoofing) which encrypts the code making sure that it is not available to unauthorized people. This is what contributes to the secret nature of the encrypted information only accessible by users with decryption keys, predominantly the U.S. military and its combined allies, ensuring its security. Also, through such arrangements, the P/Y code may remain unclipped by unauthorized replications, thus increasing the security and integrity of the Global Positioning System's military capabilities. [24], [25]

1.2.4 Positioning Principle

The positioning principle of the GPS is based on triangulation, where a GPS receiver calculates its position by measuring the distance separating it from several satellites. By knowing the distance to at least three satellites, the receiver can determine its three-dimensional position. This operation is based on electromagnetic signals emitted by the satellites, which are picked up by the receiver to calculate the position based on the information transmitted. GPS comprises three segments: the space segment (satellite constellation), the control segment (control and monitoring stations), and the user segment (GPS receivers). The satellite signals contain data on their position and time, enabling the receivers to calculate the user's position. [21], [26], [27]

1.2.5 GPS Modulation

1.2.5.1 BPSK Modulation

BPSK modulation, in which a unique method with just two symbol levels is involved and they are {+1, -1}, showing bits 1 and 0 sequentially. Through the transitions, the 180º phase difference instantly occurs. Also known by the name BPSK (β) where β denotes the spreading code rate, this modulation scheme is of utmost importance in the process of the signals' encoding and transmission. In BPSK (β = 1), +1 is for bit 1 and -1 is for bit 0. In BPSK (β = -1), -1 is for bit 1 and +1 is for bit 0.

$$S_{BPSK(\beta)}(t) = \sum_{k=-\infty}^{+\infty} a_k \, h_{T_c}(t - kT_c) \tag{1.1}$$

With:

- ak: Values (+1 or -1) of the spreading sequence
- Tc: Chip duration $T = \frac{T_0}{\beta}$ $and\ T_0 = \frac{1}{1023} ms.$
- $h\,TC(t)$ is the rectangular pulse defined by:

$$h_{T_c}(t) = \begin{cases} 1/\sqrt{Tc} & For \quad 0 < t < TC \\ 0 & ailleurs \end{cases} \tag{1.2}$$

Additionally, the BPSK Modulation is widely recognized, notably due to its prior use in the GPS system with signals from the previous generation, used to transmit the C/A and P(Y) signals. Figure 1.1 Shown the BPSK Modulation. [28], [29]

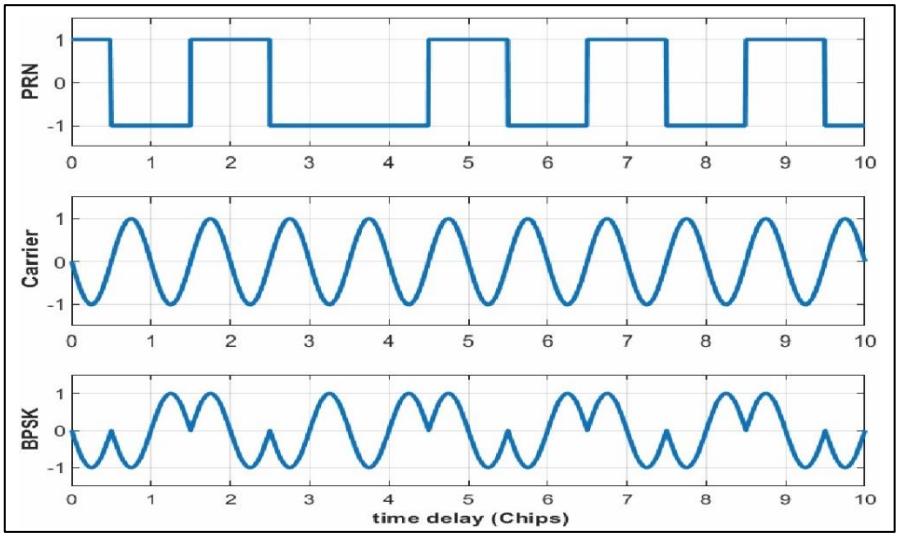

Figure 1.1 : BPSK Modulation

1.2.5.2 Autocorrelation function

The GNSS performance receivers are dependent on the corresponding frequency function between the received signals and their local replicas. This function is derived from the input signal (S(t)) and replica ($S_l(t)$), and determines the extent of signal fidelity and accuracy in the receiver's operations. Additionally, The CCF definition is Basics for extracting accurate navigation information from incoming signals. Additionally, it is important in signal processing to optimize the performance of GNSS. [28]

$$R(\tau) = \int_{-\infty}^{+\infty} S(t)S_l(t - \tau)dt \tag{1.3}$$

The formula for the Cross-Correlation Function (CCF) of BPSK-modulated signals can be represented using the variable (τ) to denote time and the shift that is applied to the locally generated code. [28]:

$$R_{BPSK}(\tau) = \begin{cases} 1 - \dfrac{|\tau|}{Tc}, |\tau| \leq T_C \\ 0, \quad ailleurs \end{cases} \tag{1.4}$$

The ACF of a BPSK-modulated signal is depicted in the Figure 1.2 , showing its general form.

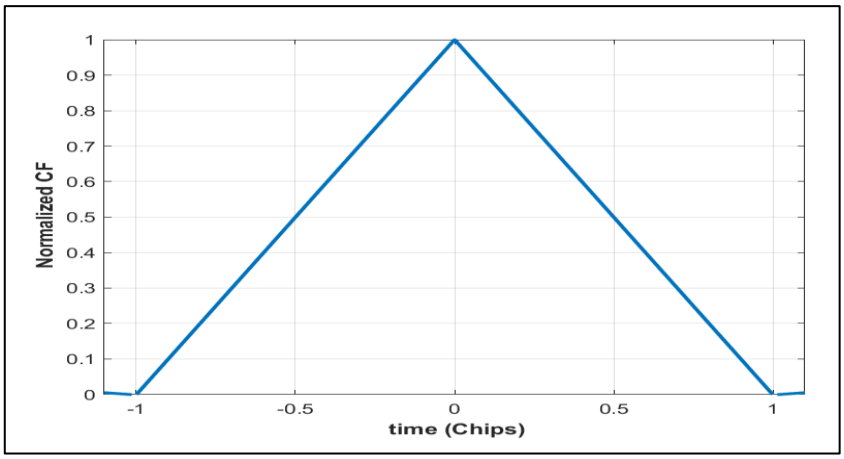

Figure 1.3 : ACF of BPSK Signal

By Figure 1.2 we can recognize the ACF shape of the BPSK signal as it is uniquely characterized by a single peak making it similar to an isosceles triangle with a base width of 2T. This peak is a visual indication of the optimal code alignment where the locally generated code matches the received signal exactly. At this point, the ACF reaches its peak, indicating maximum correlation between the transmitted and received signals.

1.2.6 Power Spectral Density

The definition of PSD is exact and is obtained by performing a Fourier transform on the ACF. This provides an understanding of how the spectral power of a signal is distributed over various frequencies. For a BPSK-modulated signal, the PSD can be represented in the following manner: [28], [29]

$$G_{BPSK}(f) = \frac{1}{f_c}\left(\frac{\sin\left(\frac{\pi f}{f_c}\right)}{\frac{\pi f}{f_c}}\right)^2 \tag{1.5}$$

In Figure 1.3, we can see the normalized signals of BPSK (1), BPSK (2), BPSK (4), and BPSK (5).

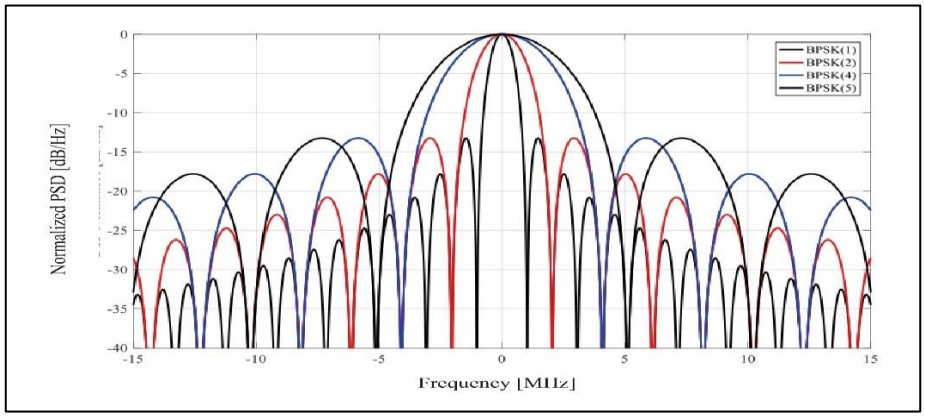

Figure 1.4 : PSDs for BPSK (1), BPSK (2), BPSK (4) and BPSK (5) codes

In addition, In Figure 1.4, the PSD of the BPSK (10) signal is presented. The majority of spectral energy in BPSK-modulated signals is centered around the main lobe, which consists of a primary lobe and several secondary lobes. The main lobe's width is twice that of the spreading code frequency.

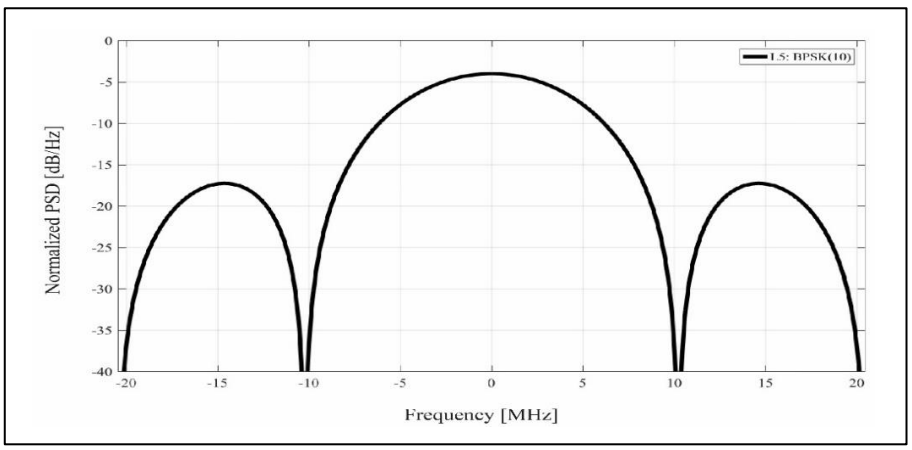

Figure 1.5 : PSD of BPSK (10) codes in GPS Band L5

1.3 Classic acquisition of GNSS signals

During the acquisition process, the received GNSS signal is synchronized with a locally generated replica. This synchronization requires the receiver to search for the frequency, phase, and delay of the PRN code of a specific satellite, which is essential for accessing navigation data. To accomplish this, the receiver must first detect which satellites are visible and obtain a rough estimate of signal parameters, such as Doppler shift (f) and code delay (τ). The phase of the D code depends on this process.

Various methods exist in the literature for conducting acquisition in GNSS applications, including serial and parallel search methods. [28], [29], [30]

1.3.1 Acquisition by Serial Search

The fundamental approach to serial search acquisition is demonstrated through Figure 1.5. The GNSS signal in digital form, named (n), is first converted to an intermediate frequency and then multiplied by a local code replica. This replica accurately reproduces the primary PRN code (n), the sub-carrier (n), and, if applicable, the secondary code $C(n)$. The outcome of this multiplication is (n), the resulting signal. [28], [31], [32]

$$S_r(t) = \sqrt{P(n)}.D(n-\tau).C(n-\tau) \times \cos(2\pi(f_{FI} + f_d)n + \emptyset_{FI}(n)) + W(n) \qquad (1.6)$$

Where:

- $P(t)$: Instantaneous power of the received signal.
- $D(t)$: Navigation data.
- (t): PRN code and subcarrier corresponding to any satellite.
- τ: Received signal delay.
- f_{FI}: Intermediate frequency.
- f_d: Doppler shift frequency corresponding to any satellite.
- $\emptyset_{FI}$: Carrier phase of the received signal.
- (t): Additive White Gaussian Noise AWGN.

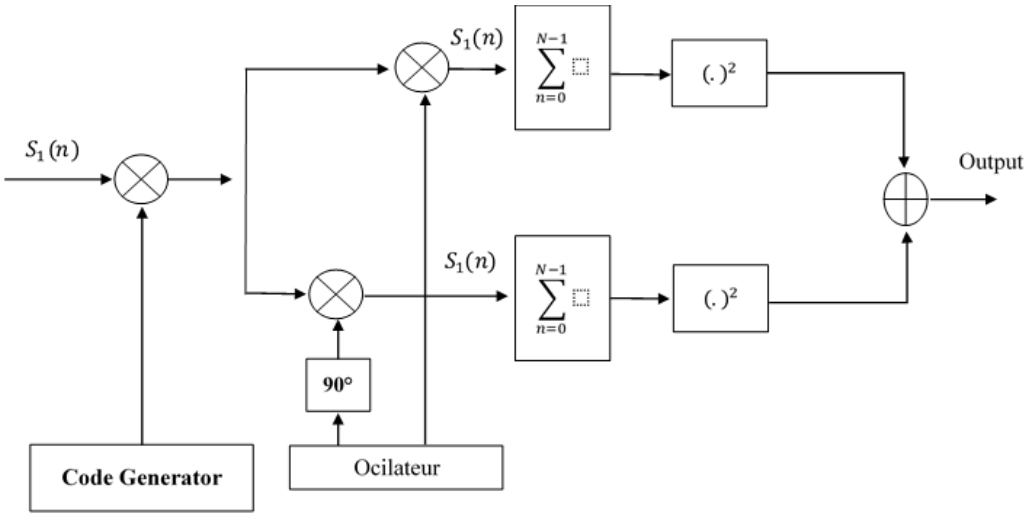

Figure 1.6 :Block Diagram of Acquisition by serial search

The delay of the local replica of the GNSS signal is represented by $\hat{\tau}$. This delay is calculated as follows: [33]

$$\hat{\tau} = \hat{\tau}_{min} + h\Delta\tau \quad pour \quad h = 0,1,2 \dots \dots . H - 1 \tag{1.7}$$

Several tests (H) are used to estimate the delay of the input signal. The input signal is then divided into two parts, namely I and Q. Finally, the two parts are multiplied to obtain the desired results. [33]

$$S_I(n, \hat{\tau}, \hat{f}_D) = S_r(n) C_1(n - \hat{\tau}) \cos(2\pi \hat{f}_D n) \tag{1.8}$$

$$S_I(n, \hat{\tau}, \hat{f}_D) = S_r(n) C_1(n - \hat{\tau}) \sin(2\pi \hat{f}_D n) \tag{1.9}$$

Multiplying the input signal by two sinusoids results in the conversion to a baseband, effectively eliminating the Doppler shift effect. Notably, the estimated Doppler frequency, denoted as "f_D," is a digital frequency. This means that it is normalized concerning the sampling frequency used by the ADC. The normalized frequency is expressed as: [33]

$$\hat{f}_D = (\hat{f}_{FI} + \hat{f}_d) T_e = \frac{f_{Fi} + \hat{f}_d}{f_e} \tag{1.10}$$

In addition, the Local Doppler frequency, chosen from a set given by:

$$\widehat{f_d} = \hat{f}_{d,min} + l\Delta \tag{1.11}$$

Where: $l = 0,1, \dots, L - 1$

To determine the frequency excursion of the incoming signal, a total of "L" different Doppler frequencies are analyzed. It is assumed that, for a stationary receiver, the frequency variation lies between: [28]

$$-10KHz \leq \widehat{f_d} \leq 10KHz$$

The signals from both branches are combined in the coherent integration block, known as Integrant and Dump. This process sums the signals over one or more code periods to obtain a correlation value, resulting in superior performance with regard to noise variance reduction. The correlators of the in-phase and quadrature branches produce outputs that can be expressed as: [33]

$$\acute{S}_I\left(n, \hat{\tau}, \widehat{f_d}\right) = \frac{1}{N}\sum_{n=0}^{N-1} S_I(n, \hat{\tau}, \widehat{f_d}) \tag{1.12}$$

$$\acute{S}_Q\left(n, \hat{\tau}, \widehat{f_d}\right) = \frac{1}{N}\sum_{n=0}^{N-1} S_Q(n, \hat{\tau}, \widehat{f_d}) \tag{1.13}$$

The coherent integration time is defined by N, which represents the number of samples used for evaluating the in-phase and quadrature components. This time is usually selected as a multiple of the period of the primary PRN code: [31]

$$T_{inc} = NT_e$$

The calculation of power in the final stage of the acquisition is done by squaring and summing the in-phase and quadrature components. Thus, the resulting output can be expressed as follows: [18]

$$S\left(n, \hat{\tau}, \widehat{f_d}\right) = \left(\acute{S}_I\left(n, \hat{\tau}, \widehat{f_d}\right)\right)^2 + \left(\acute{S}_Q\left(n, \hat{\tau}, \widehat{f_d}\right)\right)^2 \tag{1.14}$$

Where: $S\left(n, \hat{\tau}, \widehat{f_d}\right)$ is a 2-D function depending on the Doppler frequency $\widehat{f_d}$ and the delay $\hat{\tau}$.

The outcomes produced by this function are established on a two-dimensional grid, commonly known as the search space or correlation matrix. Every combination of values and corresponds to a specific time/frequency cell within the search space. [28] [30] [34]

As demonstrated in Figure 1.6, the code's time-frequency scanning principle involves a search across both time (code) and frequency (Doppler) domains.

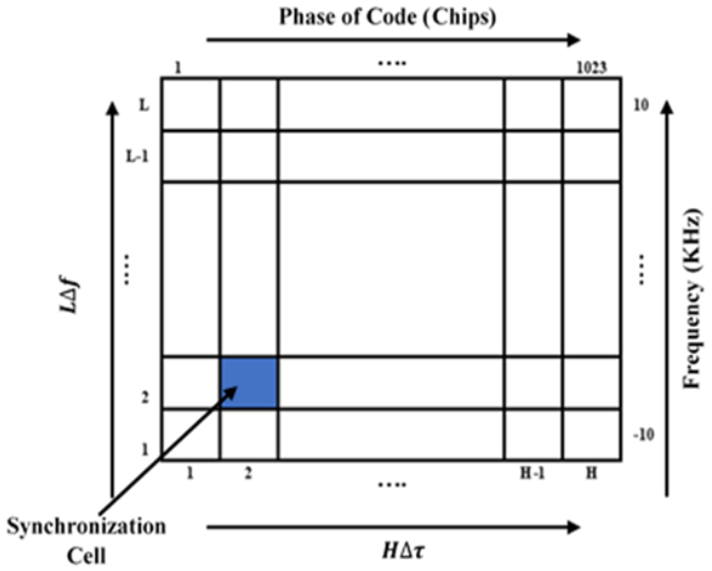

Figure 1.7 : Decalage Temporal & Frequential

Once a specific predefined threshold is reached, then we can consider the quantity $S(n, \hat{\tau}, \widehat{f_d})$ to have been acquired successfully, and at this point, values $\widehat{f_d}$ and $\hat{\tau}$ will have been estimated accurately enough. When this occurs, the satellite presence is detected by the GNSS receiver, and we can observe a correlation similar to the one displayed in Figure1.7.

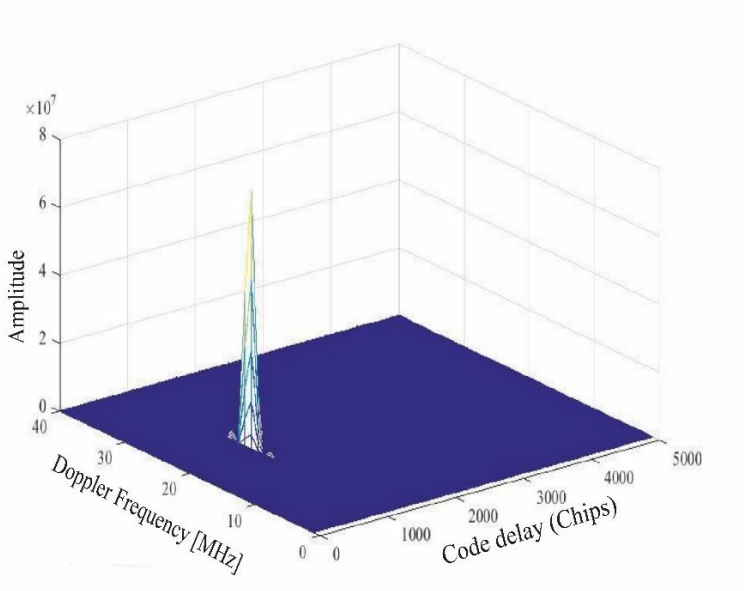

Figure 1.8 : Acquisition of GNSS Visible Satellites

The result of multiplying 1023 and 41 is equal to 41943, which indicates a relatively lengthy execution time. This further suggests a significantly heavy computational burden. [30]

1.3.2 Parallel Acquisition

The diagram in Figure 1.8 illustrates the acquisition method through parallel code search (conventional FFT method). The received digital signal $S_r(n)$ is divided into in-phase (I) and quadrature (Q) branches. The I and Q branches are then combined to form the complex signal I+Q. The real parts of $S_{e,Re}(n)$ and imaginary parts of $S_{e,Im}(n)$ are given as input to the FFT block. The output of this operation is a set of complex samples that are multiplied by the complex conjugate samples of the local code's FFT $C_1(n)$. The resulting product is then transformed into the time domain using an inverse FFT (IFFT). These transformations perform circular convolution and provide the complete correlation function over the integration period. This method calculates all possible code delays in a single operation. [35] [36]

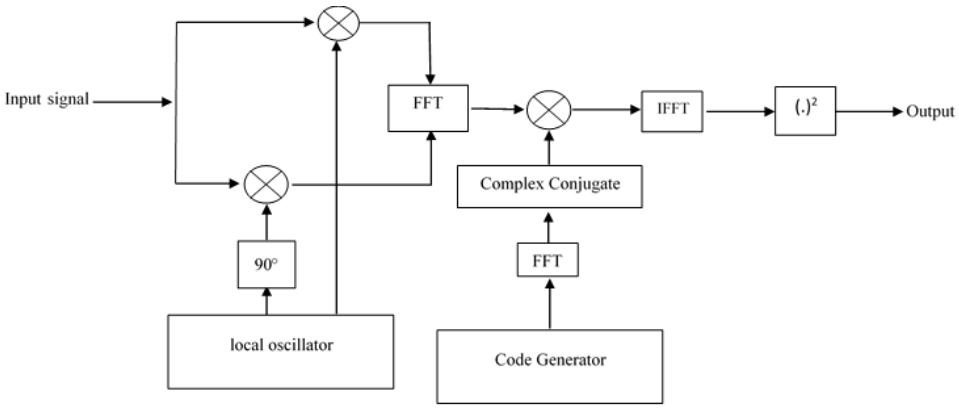

Figure 1.9 : Parallel Search Acquisition

The FFT algorithm is utilized in the correlation calculation of this acquisition system, making it faster than the serial search method. Additionally, the steps of code delay shifting are computed in parallel, further contributing to the system's efficiency.

1.4 Signal Tracking

The tracking loop operates by continually adjusting to the incoming signal, enabling the receiver to effectively de-spread and demodulate it. When the receiver is stationary, the Doppler frequency changes gradually, resulting in a low update rate for the tracking loop. To effectively track the incoming GPS signal, two tracking loops are employed: The Delay Lock Loop (DLL) and PLL [37].

The DLL is responsible for tracking the C/A code by employing early, prompt, and late code generators, along with filters and discriminators. On the other hand, the PLL is utilized to track the frequency of the incoming signal, which is directly associated with the Doppler frequency. The early and late codes are prompt codes that are time-shifted [37]

By correlating with the incoming C/A codes, the early and late codes produce two outputs that differ by half a chip or less. These outputs undergo filtering, squaring, and comparison through a discriminator. The discriminator output determines the adjustment needed for the locally generated C/A code to match that of the incoming signal. Various discriminators, such as the E-L envelope used in the current algorithm, E-L power, or E-L normalized, can be employed for this purpose. The locally generated prompt signal is then utilized to de-spread the incoming signal [37].

The Phase Lock Loop comprises a NCO, a carrier loop filter, and a discriminator. The PLL receives a signal modulated solely by the navigation message. Using the Doppler frequency calculated during the acquisition process, the NCO generates a carrier frequency [37].

The generated signal is partitioned into in-phase (I) and quadrature (Q) components. These components are then correlated with the input signal in the I and Q channels. After correlation, the outputs of the correlators undergo filtering, and the phase is examined using a discriminator. The algorithm employs an arc tangent discriminator, known for its insensitivity to phase transitions. A Phase Lock Loop utilizing this arc tangent discriminator exhibits similarities to a Costas Loop [37].

The discriminator output is employed to produce a control signal, which in turn adjusts the frequency of the oscillator (NCO). This adjustment enables the loop to consistently demodulate the incoming signal. Typically, either a second or third-order PLL can be utilized. For GPS receivers with high dynamics, it is advisable to employ a higher-order PLL. Further information on PLL can be found in [37], [38]

1.5 Pseudolite position system GPS

A pseudolite, also known as a "pseudo-satellite," is a transmitter that is situated on the ground and is capable of simulating satellite signals. It is primarily used for positioning and navigation purposes [39].

Pseudolites have been specifically developed to overcome the challenges posed by GNSS, such as GPS and Glonass, particularly in environments that are difficult to navigate, such as urban canyons, deep open-cut mines, underground areas, or indoor spaces. These locations can often interfere with or even completely block signals from satellites in space. [39]

The primary features and operations of pseudolites are as follows in Table 1.2:

Table 1.2 : features and operations of pseudolites [39]

Features and Operations	**Description**
Ground-Based Transmitters	Terrestrial transmitters are strategically installed for flexible positioning and navigation applications.
Simulation of Satellite Signals	Broadcast signals mimic those of actual satellites in GNSS constellations, including codes and frequencies similar to GPS.
Augmentation of GNSS Systems	Complement existing satellite systems by improving availability, accuracy, and reliability of positioning solutions.
Pseudolite-Only Positioning	The primary source of positioning in scenarios where satellite signals are impractical, such as indoor or underground environments.
Hardware Developments	Evolution of pseudolite hardware, including advancements in design, synchronization methods, and transceiver capabilities.
Integration with Other Technologies	Integration with sensors like Inertial Navigation Systems (INS) to enhance navigation, especially when GNSS signals are obstructed.
Challenges	Issues such as signal interference with nearby GPS receivers, the "near-far" problem, and selecting optimal frequencies.

1.6 Near/Far Problem

The problem at hand pertains to identifying the location of an object about the transmitters and its proximity to them. To better understand this, let us explore the near-far problem. Consider a hypothetical situation where two Private Land Mobiles (PLs) are constantly transmitting signals, similar to GNSS, autonomously. One of these PLs is near the user, while the other is located at a significant distance. A visual representation of this scenario can be seen in Figure 1.9. [5]

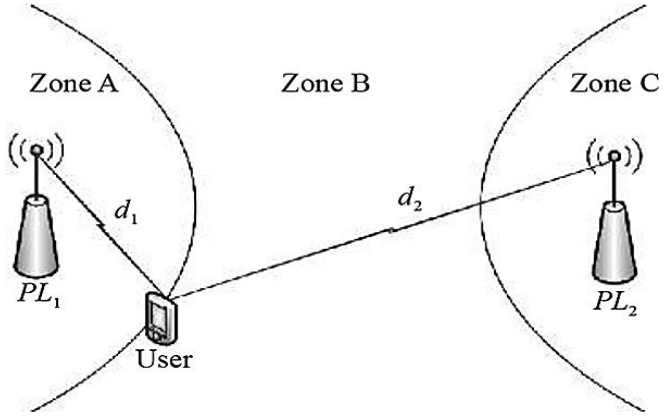

Figure 1.10 : Schematic of Receiving to PL Signal [30]

At a certain distance from PL1 and another distance from PL2, the hyperbolic curves shown in Figure 1.10 create three zones: Zone A, Zone B, and Zone C. Assuming PL transmits at a constant power level p_t, the received signal power weakens as the distance between the user and the PL increases. When the user receives a signal from PL2, the signal transmitted by PL1 can be regarded as interference. Consequently, the signal-to-interference ratio (SIR) is defined as:[5][40][41]

$$SIR = \frac{\frac{1}{{d_2}^2}\frac{1}{{d_2}^2}\,R_2(0)}{\frac{1}{{d_1}^2}\frac{1}{{d_2}^2}\,R_1(\tau)} \tag{1.15}$$

To get an equivalent fraction, you can multiply both the numerator and denominator by ${p_t}^2$ the same value.

$$SIR = \frac{\frac{1}{{d_2}^2}\frac{1}{{d_2}^2}\,R_2(0) \times {p_t}^2}{\frac{1}{{d_1}^2}\frac{1}{{d_2}^2}\,R_1(\tau) \times {p_t}^2} \tag{1.16}$$

Where: $R_2(0) = p_r$ and $p_r = \frac{p_t}{{d_2}^2} \times \alpha$ with $0 < \alpha < 1$

So:

$$SIR = \frac{\frac{1}{{d_2}^2} R_2(0) \times R_2(0) \times p_t}{\frac{1}{{d_1}^2} R_1(\tau) \times R_1(\tau) \times p_t} \tag{1.17}$$

Finally:

$$SIR = \frac{\frac{1}{{d_2}^2} |R_2(0)|^2}{\frac{1}{{d_1}^2} |R_1(\tau)|^2} = \frac{{d_1}^2 |R_2(0)|^2}{{d_2}^2 |R_1(\tau)|^2} \tag{1.18}$$

The auto-correlation values, $R_2(0)$, and cross-correlation values of pseudo random codes, $R_1(\tau)$, are used to evaluate GNSS C/A codes composed of Gold sequences. These sequences are characterized by their normalized cross-correlation over a code period $N = 2^n - 1$, which can be described by three distinct functions. [42]

where:

$$\left\{\frac{\beta(n) - 2}{N} ; \frac{1}{N} ; \frac{-\beta(n)}{N}\right\} \tag{1.19}$$

$$\beta(n) = 1 + 2^{1+\left\lfloor\frac{n}{2}\right\rfloor} \tag{1.20}$$

We can obtain the SIR bound from Eq 1.18 and 1.20, where denotes the greatest integer that is less than or equal to: [5]

$$SIR = \frac{{d_1}^2 |R_2(0)|^2}{{d_2}^2 |R_1(\tau)|^2} \geq \left|\frac{2^n - 1}{1 + 2^{\left\lfloor\frac{(n+2)}{2}\right\rfloor}}\right|^2 \times \left|\frac{d_1}{d_2}\right|^2 \tag{1.21}$$

We define the near-far ratio by setting the maximum value for the worst scenario as $|R_1(\tau)| = \beta(n)$. In this scenario, we consider the near-far ratio as follows: [5]

$$l \triangleq \frac{d_1}{d_2} \tag{1.22}$$

To maintain stable tracking, most receivers require a minimum SIR of 6 dB. This implies that the SIR must exceed this value. For instance, taking the C/A codes used in the navigation system as a reference (), we can derive the near-far ratio from Eq 1.21 and 1.22. [5]

$$l \leq \frac{2^n - 1}{2^{\lfloor (n+2) \div 2 \rfloor} + 1} / 10^{0.3} \approx 7.9 \tag{1.23}$$

According to Eq 1.23, the maximum near-far ratio is 7.9, meaning that if the distance between the user and the two PLs is more than 7.9 times, the near PL signal willfully interfere with the user receiver, resulting in abnormal operation. For example, referring to Figure 1.10, the receiver can only function properly in zone B, which is a limited area. It can only receive signals in zone A, and not in zone C [5].

As the number of PLs increases, the range of the receiver's ability to track all desired PL signals will decrease. To address this near-far effect, pulse modulation of the conventional DSSS signal can be used, along with the adoption of the new spreading code of good cross-correlation, as discussed below [5] [42].

1.7 Solution of Problem (Near/Far)

To solve the issue of near-far interference, several methods have been put forward. These can be broadly categorized into three groups - signal pulses, frequency shifts, and the utilization of different PRN codes. Frequency shift techniques involve transmitting Pseudolite signals on a carrier frequency that is different from the GPS L1 carrier frequency. This approach necessitates adjustments to the receiver's front end to accommodate the frequency shift. Van Dierendonck and Elrod proposed a method in 1993 that places the Pseudolite signal on the first zero of GPS satellite signals, which is a 1,023 MHz shift from the L1 frequency. However, this technique requires significant changes to the receiver design. Previous methods to tackle near-far interference entail modifying the transmitter or the transmitted signal to reduce the impact on GPS. Successive Interference Cancellation (SIC) is a technique applied at the receiver's signal processing stage to mitigate the effects of GPS-like transmissions on ambient noise power. SIC has been used to attenuate the near-far dilemma in IS-95 cellular systems. This approach is well-suited for software or digital receiver designs based on signal processing, where multiple channels can be leveraged in parallel with significant signal processing capacity [43].

CDMA-based ad hoc networks use a combination of open- and closed-loop power control to address the near-far problem. This ensures that each mobile terminal generates the same signal power at the base station. The base station monitors the received signal power from each terminal and instructs distant terminals to increase their signal power while nearby terminals decrease theirs. However, this same solution cannot be applied to mobile ad hoc networks (MANETs) due to the medium access problem. In MANETs, the solution to the near-far problem must have both power control and medium access elements. To address this issue in GPS and CDMA-based systems, various methods have been proposed, including frequency shifts, power control, and medium access techniques. The choice of method depends on the specific system and application requirements. [43]

1.8 Conclusion

In this chapter, we present the GPS and Pseudolite system. We introduce GPS segments and codes, followed by a detailed study of BPSK modulation and GPS signal acquisition. Finally, we give a general overview of the Pseudolite GPS system, its near-far problem and its solution.

Chapter 2 :

Time Hopping Pseudolite's SIT generation

2.1 Introduction

In the field of global navigation, PLs serve as ground-based transmitters that enhance GNSS signal availability in areas where GNSS satellites are not accessible. They can create self-contained local positioning systems, taking the place of GNSS satellites. However, they have the potential to disrupt weak signals at the receiving end with near-far interference. To tackle this issue, TH pulsed PL signals are seen as an effective solution.

TH signals are produced by gating continuous GNSS-like signals with TH pulses that are regulated by SIT. Creating a well-designed SIT involves using pseudo-random THSIs, matching spreading factors with original signals, and allocating distinct SITs to each PL to enable receiver discrimination.

In this Chapter, we present a novel approach for developing SITs for PLs. Our method involves constructing different THSI base matrices using congruence codes. These matrices are then merged, and specific rows are chosen to create SITs. This allows for the creation of diverse SITs for various PLs by modifying the combined matrices.

2.2 Time hopping

2.2.1 Signal model

The equation used to generate the TH pulsed signal was as follows [44]:

$$g(t) = \sum_{n=-\infty}^{+\infty} \sum_{k=0}^{\Gamma N_s - 1} uT_P(t - n\Gamma T_b - kT_c - a_k^{(n)} T_c d) \tag{2.1}$$

The TH pulses that contain the GNSS signal are multiplied together in this equation to create a sum. [44]

Where: $uT_P(t)$ is the rectangle of TH pulse [44].

$$uT_p(t) = \begin{cases} 1 \; if & 0 < t < T_P \\ 0 & otherwhise \end{cases} \tag{2.2}$$

T_b and T_c are periods of data bit and PRN code sequence of the original GNSS-like signal, also the duty cycle of TH pulse is d .Moreover the duration of TH pulse is $T_p \triangleq T_c \times d$, and the period repetitions of PRN code in one GNSS-like signal data bit period is [44]:

$$N_s = {}^{T_b}/_{T_c}$$

Γ is The ratio of bit periods between the Pseudo-Lite PL signal and the original GNSS signal.

Where: N_f is the total slot number in one TH frame [44]:

$$N_f \triangleq {}^{1}/_{d}$$

In the nth PL data bit, the value $\left\{a_k^{(n)}\right\}_{k=0}^{\Gamma N_s-1}$ in the kth slot represents the THIS which are indices used to control the positions of TH pulses in the PL signal. These TH pulses are used to gate the continuous local-generated GNSS-like signal. THSIs are organized into permutation sequences within a SIT, which determines the timing and sequence of the TH pulses [3][4] [44].

The values of THSIs is chosen randomly from the set $\{0, 1, \ldots., N_f - 1\}$, where N_f is a parameter that defines the length of the SIT [44].

Table 2.1 :The Th Table used to Generate and detect the TH slot indices of the pseudolite signal [3]

Group ID	**TH slot index in different frame(0_k-1) of one basic pulse pattern**				
	0	**1**	**2**	**….**	**K-1**
1	$a_0^{(1)}$	$a_1^{(1)}$	$a_2^{(1)}$	….	$a_{\mathbf{K-1}}^{(1)}$
2	$a_0^{(2)}$	$a_1^{(2)}$	$a_2^{(2)}$	…..	$a_{\mathbf{K-1}}^{(2)}$
⋮	⋮	⋮	⋮	⋮	⋮
$\boldsymbol{v-1}$	$a_0^{(v-1)}$	$a_1^{(v-1)}$	$a_2^{(v-1)}$	….	$a_{\mathbf{K-1}}^{(v-1)}$
$\boldsymbol{v}$**(used)**	$a_0^{(v)}$	$a_1^{(v)}$	$a_2^{(v)}$		$a_{\mathbf{K-1}}^{(1)}$
$\boldsymbol{v}$**+1**	$a_0^{(v+1)}$	$a_0^{(v+1)}$	$a_0^{(v+1)}$	….	$a_{\mathbf{K-1}}^{(1)}$
⋮	⋮	⋮	⋮	⋮	⋮
$\boldsymbol{N}$	$a_0^{(N)}$	$a_1^{(N)}$	$a_2^{(N)}$	….	$a_{\mathbf{K-1}}^{(N)}$

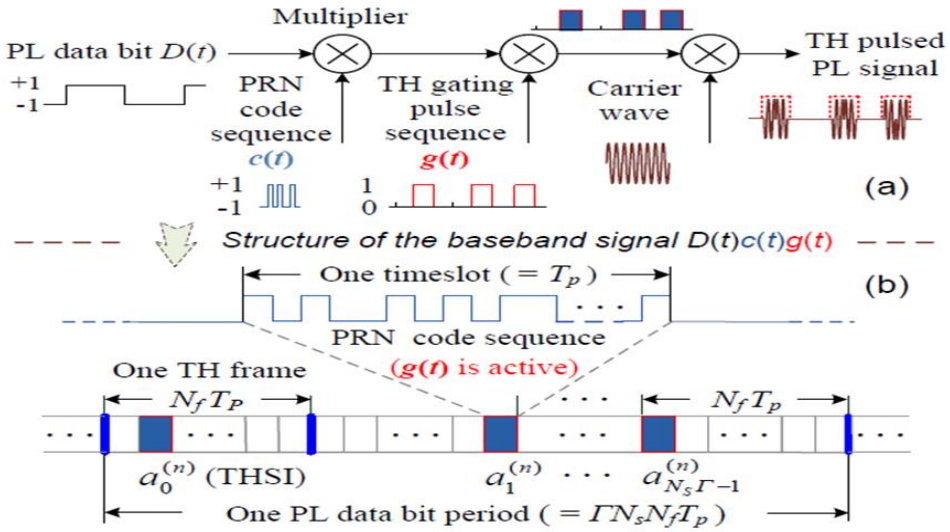

Figure 2.1 :Generation of The TH pulsed PL Signal in which (a) the Schematic and (b) the stricture of baseband signal [44]

2.2.2 Slot Index Table

The SIT is a fundamental component used in the generation of TH pulsed PL signals. It is crucial for maintaining the spectral shape of the original GNSS-like signal, ensuring compatibility and integrity. Additionally, each PL is assigned a different SIT, allowing receivers to distinguish between various PLs besides using PRN codes of the underlying GNSS-like signal like the Table

As illustrated in the Table 2.1, this table consists of multiple permutation sequences of THSIs. These THSIs determine the positions of the TH pulses that gate the continuous local-generated GNSS-like signal, thereby realizing the TH pulsed PL signal [44].

2.3 SLOT index table generation

2.3.1 Generated by Locata Schemes

The TDMA scheme for PLs divides each millisecond into 10 time slots of 900 microseconds, forming a TDMA frame, with 200 frames making up a 200-millisecond super frame. PLs operating in a time slot are divided into geographical sub-networks of up to 10 PLs, with non-overlapping assigned time slots. Each PL transmits during its assigned slot, while the others remain silent, and assignments vary randomly from frame to frame to reduce interference. Up to 5 separate sub-networks can be defined for a time slot, allowing up to 50 PLs per slot, with schemes designed to minimize overlap and interference between sub-networks, requiring geographical separation or other isolation measures to ensure optimum performance. [4]

Table 2.2 :Assigning TDMA Slot to the location number [4]

TDMA Frame	**Timeslot within Frame (slot sequence number)**									
	1	**2**	**3**	**4**	**5**	**6**	**7**	**8**	**9**	**10**
181	1	8	7	3	4	10	6	9	2	5
182	7	4	10	5	9	3	2	6	1	8
183	9	5	1	6	7	8	4	3	10	2
184	4	9	5	2	7	6	8	10	3	1
185	10	7	9	4	2	1	3	5	8	6
186	5	6	7	8	3	2	4	1	9	10
187	6	9	1	2	8	4	7	3	10	5
188	1	7	4	6	5	10	3	8	2	9
189	7	2	8	10	6	3	1	5	4	9
190	6	8	3	7	1	2	5	10	9	4
191	5	1	6	4	9	8	7	2	10	3
192	8	5	10	1	4	2	6	9	3	7
193	1	4	3	7	5	9	2	8	6	10
194	8	10	5	6	2	9	1	3	4	7
195	3	5	4	8	1	10	2	7	9	6
196	4	10	7	9	8	5	2	3	6	1
197	7	6	10	5	2	3	9	4	1	8
198	2	10	4	3	6	1	9	5	7	8
199	5	3	1	10	9	7	8	2	4	6
200	2	1	9	5	8	7	10	4	6	3

2.4 Generation of THSI Base Matrices and Different SITs

2.4.1 Construction of the Congruence Codes

To generate this THISs should be constricted by the Congruence Codes [44] [46] [47]:

$$x_{i,j}^{(l)} = (\frac{(i+1)(j+1)}{l} - 1)(mod\ p) \tag{2.3}$$

- p is the prime number i, j and l are all integer.

$0 < i, j < p - 2$ and $1 < l < p - 1$

Then, through the modular multiplicative inverse operation, it can be readily deduced that [46] [47]:

$$x_{i,j}^{(l)} \epsilon \{0,1, \dots \dots \dots . . p - 2\}$$

2.4.2 Generation of THSI Base Matrices

So, the matric was be like that [1]:

$$X^l = \begin{bmatrix} x_{0,0}^{(l)} & x_{0,1}^{(l)} & x_{0,2}^{(l)} & x_{0,3}^{(l)} \\ x_{1,0}^{(l)} & x_{1,1}^{(l)} & x_{1,2}^{(l)} & x_{1,3}^{(l)} \\ x_{2,0}^{(l)} & x_{2,1}^{(l)} & x_{2,2}^{(l)} & x_{2,3}^{(l)} \\ x_{3,0}^{(l)} & x_{3,1}^{(l)} & x_{3,2}^{(l)} & x_{3,3}^{(l)} \end{bmatrix}$$

So, for example to determine $X^{(1)}\ X^{(2)}$ with $N_f = 4$ we should calculus all that element of $x_{i,j}^{(1,2)}$with:

$$X^1 = \begin{bmatrix} 0 & 1 & 2 & 3 \\ 1 & 3 & 0 & 2 \\ 2 & 0 & 3 & 1 \\ 3 & 2 & 1 & 0 \end{bmatrix} \ ; X^2 = \begin{bmatrix} 2 & 0 & 3 & 1 \\ 0 & 1 & 2 & 3 \\ 3 & 2 & 1 & 0 \\ 1 & 3 & 0 & 2 \end{bmatrix}$$

We set $x_{i1}^{(l)}$ is the first row from $X^{(l)}$ and $x_{i2}^{(l)}$ the second-row sow where $i_1 \neq i_2$ we define:

$x_{i2,\tau}^{(l)} =\triangleq [x_{i2,1\oplus\tau}^{(l)}, x_{i2,1\oplus\tau}^{(l)}, x_{i2,1\oplus\tau}^{(l)} \qquad x_{i2,1\oplus\tau}^{(l)}]$ where τ is cyclic shift $0 < \tau < N_f, \tau \epsilon \mathbb{Z}$

2.4.2.1 Theorem 1

The hit number of THSIs between $x_{i1}^{(l)}$and $x_{i2,\tau}^{(l)}$ is at most one where $0 < \tau < N_f, \tau \epsilon \mathbb{Z}$[44]

- **Proof:**

We take $x_{i1}^{(1)} = [0\ 1\ 2\ 3\ ]$ and $x_{i2}^{(1)} = [1\ 3\ 0\ 2]$ $x_{i2,\tau}^{(1)}$ =[2 1 3 0]

The hit number between $x_{i1}^{(1)} = [0\ 1\ 2\ 3\ ]$ and $x_{i2,\tau}^{(1)}$ =[2 1 3 0] is one number in the second index.

Suppose there are two hits between $x_{i1}^{(1)}$and $x_{i2,\tau}^{(1)}$then from (2.1)it can be derived that[44][46]

$$(i_1 + 1) \otimes (j_1 + 1) = (i_2 + 1) \otimes \left((j_1' + 1) \oplus \tau\right) \quad (2.4)$$

$$(i_1 + 1) \otimes (j_2 + 1) = (i_2 + 1) \otimes \left((j_2' + 1) \oplus \tau\right) \quad (2.5)$$

Must hold simultaneously, where $j_1 \neq j_2,\ j_1' \neq j_2'$ and $j_1 - j_2 = j_1' - j_2'$ $\otimes$ denotes a modulo-N_f multiplication.

By subtracting (3) and (4) it is easily derived that $i_1 = i_2$ .this result will contradict the assumption $i_1 \neq i_2$so there is at most one hit between $x_{i1}^{(1)}$and $x_{i2,\tau}^{(1)}$ the same conclusion can be drawn for any two distinct columns of $X^{(l)}$.

2.4.2.2 Theorem 2

The hit number of THSIs between $x_{i1}^{(l)}$ and $x_{i2,\tau}^{(l')}$ where $l' \neq l$ which come from $X^{(l)}$ [44]

$X_{\tau}^{(l')}$ respectively, is at most N_f where $0 < i_1, i_2 < N_f - 1$ $1 < l\ , l' < N_f$ $0 < \tau < N_f, \tau \epsilon \mathbb{Z}$

- **Proof:**

We take $x_{i1}^{(1)} = [0\ 1\ 2\ 3\ ]$ and $x_{i2}^{(2)} = [3\ 2\ 1\ 0\ ]$ $x_{i2,\tau}^{(2)}$ =[0 3 2 1] , $\tau = 1$

The hit number between $x_{i1}^{(1)} = [0\ 1\ 2\ 3\ ]$ and $x_{i2,\tau}^{(2)}$ =[0 3 2 1] is tow in first index and the third index.

By subtracting (2.4) with (2.5) again after changing l to l' in the right terms of these tow equations ,it can be derived that $(i_1+1)\otimes(1/l)=(i_2+1)\otimes(1/l')$ will hold under $i_1+1=l$ and $i_2+1=l'$, and this implies that $x_{i1}^{(l)}$ may fully hit $x_{i2,\tau}^{(l')}$ or cause N_f hits . on the other hand if $(i_1+1)\otimes(1/l)\neq(i_2+1)\otimes(1/l')$ then only one of equation (3) and (4) will hold and this means the hit number between $x_{i1}^{(l)}$ and $x_{i2,\tau}^{(l')}$is not more than one thus the THSI hit number between $x_{i1}^{(l)}$ and $x_{i2,\tau}^{(l')}$ is at most under and $0<\tau<N_f, \tau\epsilon\mathbb{Z}$

2.5 Generation of Different SITs by combining different base matrices

To generate a different SITs for different PLs we propose this method which is represented by combining a different base matrices N ,so the number of THISs in one SIT is $\Gamma\, T_b/T_c$, And in matrix $X^{(l)}$ is N_f^2 so to determine N or number of matrices we divide the number of THISs in one SIT on the number of THISs in one matrix $X^{(l)}$as that:

$$1matrix \rightarrow N_f^2(THSIs)$$

$$N = ? \rightarrow \Gamma T_b/T_c$$

So, the total number of THSIs from matrices for a SIT ($\Gamma\, T_b/T_c$) is NN_f^2 and finally we define N :

$$N = \left\lceil \Gamma\, T_b/(T_c N_f^2) \right\rceil$$

The number of THSIs in row for combining N matrices is K, For example suppose:

$\mathrm{T_b} = 20\mathrm{ms}$, $\mathrm{T_c} = 1\mathrm{ms}$, $\Gamma = 10$, $\mathrm{d} = 0.1$ $\mathrm{N}_f = 10$ [4] [44]

From these values we derived:

$\Gamma\ \mathrm{T_b}/\mathrm{T_c} = 2\mathrm{OO}$, $\mathrm{N} = 2$, $\mathrm{K} = 10$

Sow hear to generate this SIT we combining 2 matrices:

$$X^{l}=\begin{bmatrix}0&1&2&3&4&5&6&7&8&9\\1&3&5&7&9&0&2&4&6&8\\2&5&8&0&3&6&9&1&4&7\\3&7&0&4&8&1&5&9&2&6\\4&9&3&8&2&7&1&6&0&5\\5&0&6&1&7&2&8&3&9&4\\6&2&9&5&1&8&4&0&7&3\\7&4&1&9&6&3&0&8&5&2\\8&6&4&2&0&9&7&5&3&1\\9&8&7&6&5&4&3&2&1&0\end{bmatrix} \quad ; \quad X^{l'}=\begin{bmatrix}5&0&6&1&7&2&8&3&9&4\\0&1&2&3&4&5&6&7&8&9\\6&2&9&5&1&8&4&0&7&3\\1&3&5&7&9&0&2&4&6&8\\7&4&1&9&6&3&0&8&5&2\\2&5&8&0&3&6&9&1&4&7\\8&6&4&2&0&9&7&5&3&1\\3&7&0&4&8&1&5&9&2&6\\9&8&7&6&5&4&3&2&1&0\\4&9&3&8&2&7&1&6&0&5\end{bmatrix}$$

We get:

$X_K^{(l,l')}$=$\left[X^{(l)}\ X^{(l')}\right]$ with $K \leq N_f$

$$X_K^{(l,l')} = \begin{bmatrix} 0 & 1 & 2 & 3 & 4 & 5 & 6 & 7 & 8 & 9 & 5 & 0 & 6 & 1 & 7 & 2 & 8 & 3 & 9 & 4 \\ 1 & 3 & 5 & 7 & 9 & 0 & 2 & 4 & 6 & 8 & 0 & 1 & 2 & 3 & 4 & 5 & 6 & 7 & 8 & 9 \\ 2 & 5 & 8 & 0 & 3 & 6 & 9 & 1 & 4 & 7 & 6 & 2 & 9 & 5 & 1 & 8 & 4 & 0 & 7 & 3 \\ 3 & 7 & 0 & 4 & 8 & 1 & 5 & 9 & 2 & 6 & 1 & 3 & 5 & 7 & 9 & 0 & 2 & 4 & 6 & 8 \\ 4 & 9 & 3 & 8 & 2 & 7 & 1 & 6 & 0 & 5 & 7 & 4 & 1 & 9 & 6 & 3 & 0 & 8 & 5 & 2 \\ 5 & 0 & 6 & 1 & 7 & 2 & 8 & 3 & 9 & 4 & 2 & 5 & 8 & 0 & 3 & 6 & 9 & 1 & 4 & 7 \\ 6 & 2 & 9 & 5 & 1 & 8 & 4 & 0 & 7 & 3 & 8 & 6 & 4 & 2 & 0 & 9 & 7 & 5 & 3 & 1 \\ 7 & 4 & 1 & 9 & 6 & 3 & 0 & 8 & 5 & 2 & 3 & 7 & 0 & 4 & 8 & 1 & 5 & 9 & 2 & 6 \\ 8 & 6 & 4 & 2 & 0 & 9 & 7 & 5 & 3 & 1 & 9 & 8 & 7 & 6 & 5 & 4 & 3 & 2 & 1 & 0 \\ 9 & 8 & 7 & 6 & 5 & 4 & 3 & 2 & 1 & 0 & 4 & 9 & 3 & 8 & 2 & 7 & 1 & 6 & 0 & 5 \end{bmatrix}$$

2.6 Correlation Property Analysis of the Formed SIT

2.6.1 Binary Mapping of the Formed SIT:

To generate signal PL, we need to assign signal SIT, which is formed into a binary code and assigned a correlation property, which is the easiest way to characterise the hit property. To accomplish this work, we take a K rows from $X_K^{(l,l')}$, the size of this is $K2N_f$ and we concatenated sequentially to form an array.

$$a_{SIT}^{(l,l')} = \left[a_0^{(l,l')}, a_1^{(l,l')}, \ldots\ a_k^{(l,l')}\ \ldots\ldots\ldots\ldots a_{K2N_f-1}^{(l,l')}\right]$$

Then this $a_{SIT}^{(l,l')}$ is mapped into binary code sequence:

$$\left\{\vartheta_i^{(l,l')}\right\}_0^{K2N_f{}^2-1}$$

$$\vartheta_i^{(l,l')} = \begin{cases} 1, i = a_k + kN_f, k \in \mathbb{z}, 0 \leq k \leq K2N_f - 1 \\ 0\ otherwise \end{cases} \quad (2.6)$$

So $a_{SIT}^{(l,l')}$ is just $\left\{a_k^{(n)}\right\}_0^{\Gamma N_s-1}$ the size of $a_{SIT}^{(l,l')}$ is $K2N_f$ and $\left\{a_k^{(n)}\right\}_0^{\Gamma N_s-1}$ is $\Gamma\ N_s$

$K2N_f = \Gamma\ N_s$ with $\Gamma = K$, $2N_f = N_s$

From (4), we can get the size of: $\vartheta_i^{(l,l')}$ $0 \leq i \leq K2N_f{}^2 - 1$ is $K2N_f{}^2$

- **Example**:

We have:

$$a_{SIT}^{(l,l')} = \begin{bmatrix} 0 & 1 & 2 & 3 & 4 & 5 & 6 & 7 & 8 & 9 & 5 & 0 & 6 & 1 & 7 & 2 & 8 & 3 & 9 & 4 \\ 1 & 3 & 5 & 7 & 9 & 0 & 2 & 4 & 6 & 8 & 0 & 1 & 2 & 3 & 4 & 5 & 6 & 7 & 8 & 9 \\ 2 & 5 & 8 & 0 & 3 & 6 & 9 & 1 & 4 & 7 & 6 & 2 & 9 & 5 & 1 & 8 & 4 & 0 & 7 & 3 \\ 3 & 7 & 0 & 4 & 8 & 1 & 5 & 9 & 2 & 6 & 1 & 3 & 5 & 7 & 9 & 0 & 2 & 4 & 6 & 8 \\ 4 & 9 & 3 & 8 & 2 & 7 & 1 & 6 & 0 & 5 & 7 & 4 & 1 & 9 & 6 & 3 & 0 & 8 & 5 & 2 \\ 5 & 0 & 6 & 1 & 7 & 2 & 8 & 3 & 9 & 4 & 2 & 5 & 8 & 0 & 3 & 6 & 9 & 1 & 4 & 7 \\ 6 & 2 & 9 & 5 & 1 & 8 & 4 & 0 & 7 & 3 & 8 & 6 & 4 & 2 & 0 & 9 & 7 & 5 & 3 & 1 \\ 7 & 4 & 1 & 9 & 6 & 3 & 0 & 8 & 5 & 2 & 3 & 7 & 0 & 4 & 8 & 1 & 5 & 9 & 2 & 6 \\ 8 & 6 & 4 & 2 & 0 & 9 & 7 & 5 & 3 & 1 & 9 & 8 & 7 & 6 & 5 & 4 & 3 & 2 & 1 & 0 \\ 9 & 8 & 7 & 6 & 5 & 4 & 3 & 2 & 1 & 0 & 4 & 9 & 3 & 8 & 2 & 7 & 1 & 6 & 0 & 5 \end{bmatrix}$$

so, the first value $a_0^{(l,l')} = 0$ its mean we take the first frame and $a_1^{(l,l')}$ its mean we take the second frame this value of $a_{SIT}^{(l,l')}$ represent the order or wich frame used of TH PL signal

Table 2.3 :The Value of i when $\vartheta = 1$

$a_{SIT}^{(l,l')}$	$a_0^{(l,l')}$	$a_1^{(l,l')}$	$a_2^{(l,l')}$	$a_3^{(l,l')}$	$a_{199}^{(l,l')}$
i	0	11	22	33 ……	1995

This flowchart shows the stages of generating a SIT

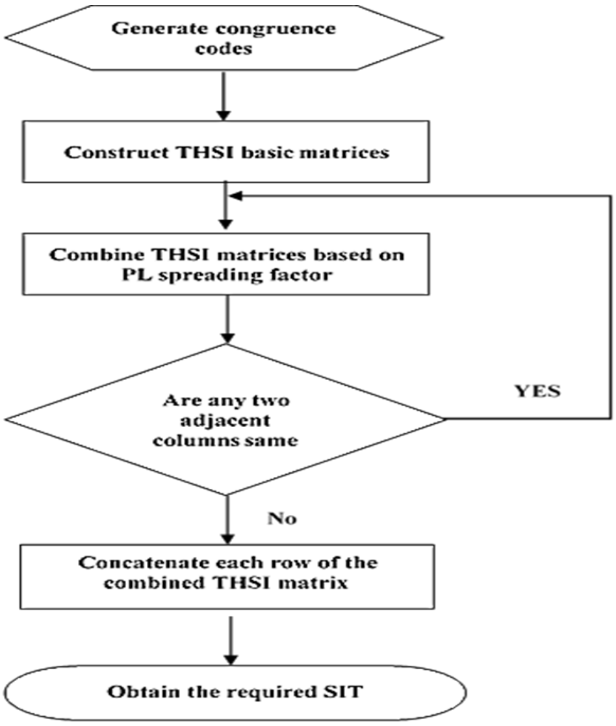

Figure 2.2 ; flow chart of generating one SIT of TH pulsed PL.

2.6.2 Auto- and Cross-Correlation Properties of the Formed SIT

With the obtained sequence $\left\{\vartheta_i^{(l,l')}\right\}_0^{K2N_f{}^2-1}$ the correlation properties of the formed SIT can be evaluated by ACF and CCF [45]

$$\left\{\vartheta_i^{(l,l')}\right\}_0^{K2N_f{}^2-1}$$

$$R_{\vartheta^{(l,l')}}(\tau) = \sum_{i=0}^{2KN_f^2-1} \vartheta_i^{(l,l')}\, \vartheta^{(l,l')}_{(i+\tau)mod\left(2KN_f^2\right)} \tag{2.7}$$

$$C_{\vartheta^{(l,l')}}(\tau) = \sum_{i=0}^{2KN_f^2-1} \sum_{\substack{j=0,\\ j\neq i}}^{2KN_f^2-1} \vartheta_i^{(l,l')}\, \vartheta^{(l,l')}_{(j+\tau)mod\left(2KN_f^2\right)} \tag{2.8}$$

respectively, where τ is the cyclic shift of the mapped code sequence $\tau \in \mathbb{Z}$ and $0 \le \tau \le 2KN_f^2 - 1$ For convenience, here the right shift of τ is chosen for analysis Then based on (7) and (8) and Theorems 1 and 2, the properties of $R_{\vartheta^{(l,l')}}(\tau)$ and $C_{\vartheta^{(l,l')}}(\tau)$ can given as follows :

2.6.2.1 Theorem 3

The subpeak upper bound of $R_{\vartheta^{(l,l')}}(\tau)$ normalised to $R_{\vartheta^{(l,l')}}(0)$ equal $(N_f + K - 1)/(KN_f)$

Where $\tau \in \mathbb{Z}$ and $0 \le \tau \le 2KN_f^2 - 1$.

2.6.2.2 Corollary 1

The subpeak upper bound of $C_{\vartheta^{(l,l')}}(\tau)$ normalised to $R_{\vartheta^{(l,l')}}(0)$ equal $(N_f + 2K - 2)/(KN_f)$

Where $\tau \in \mathbb{Z}$ and $0 \le \tau \le 2KN_f^2 - 1$.

- **Proof:**

the subpeak upper bound of $R_{\vartheta^{(l,l')}}(\tau)$ it is easily to get equals the maximum hit number between $\left\{\vartheta_i^{l,l'}\right\}_0^{2KN_f^2-1}$ and it is τ cyclic shift result.

$\xi_r \triangleq \lfloor \tau/2N_f^2 \rfloor$ $\xi_h \triangleq \lfloor \tau/N_f^2 \rfloor$ $\xi_f \triangleq \lfloor \tau/N_f \rfloor$ $c \triangleq \xi_f N_f$ $\tau_e \triangleq \tau(mod\ N_f)$

Let $x_{i_\gamma,j}^{(l_1,l_2)}$ and $x_{u,v}^{(l_1,l_2)}$ be the elements of $X_K^{(l,l')}$ and its equivalent τ cyclic shift result $X_{K,\tau}^{(l,l')}$

Where $i_\gamma, \gamma, u, v, j$are all integer and they meet $0 \le i_\gamma, u \le N_f - 1$, $0 \le \gamma \le K - 1$

$0 \le v, j \le 2N_f - 1$ Then the previous maximum hit number also equals the maximum hit result between $X_K^{(l,l')}$ and $X_{K,\tau}^{(l,l')}$ when τ takes a certain value and the following

relationships are satisfied $u = i_{\gamma\oplus\xi_r}, v = \left(j + \xi_f\right)\left(mod\ 2N_f\right)$ and $x_{u,v}^{(l_1,l_2)} = x_{i_\gamma,j}^{(l_1,l_2)} \oplus \tau_e$

Based on this idea, the hits between $X_K^{(l,l')}$ and $X_{K,\tau}^{(l,l')}$ under different τ and above relationship

Can be first given as follows.

1)When $\tau = 2\eta N_f^2$ where $\eta \in \mathbb{N}$ and $1 \le \eta \le K-1$, the parameter $\tau_f = \tau$ and $\tau_e = 0$

At this time $X_{K,\tau}^{(l,l')}$ can be written as $X_{K,\tau}^{(l,l')} = \left[X_{K,\xi_r}^{(l)}\ X_{K,\xi_r}^{(l')}\right]$, where

$X_{K,\xi_r}^{(l)} = \left[x_{\xi_r,0}^{(l)}\ \ x_{\xi_r,1}^{(l)}\ \ x_{\xi_r,m}^{(l)}\ \ \ x_{\xi_r,(N_f-1)}^{(l)}\right]$ in which $x_{\xi_r,m}^{(l)} = \left[x_{i_{\xi_r},m}^{(l)}\ \ x_{i_{\xi_r\oplus 1},m}^{(l)}\ x_{i_{\xi_r\oplus(K-1)},m}^{(l)}\right]$

$$m = 0,1,\ldots N_f - 1$$

From theorem 1 the total hits between $X_{K,\xi_r}^{(l)}, X_{K,}^{(l)}$ are at most K then from that we set the total hits between $X_{K,\tau}^{(l,l')}\ X_K^{(l,l')}$are at most $2K$,when $\tau = (2\eta-1)N_f^2$ where $\eta \in \mathbb{N}$ and $1 \le \eta \le K$, the parameter $\tau_f = \tau$ and $\tau_e = 0$.

From theorem 2 the cross hits between $X_{K,\xi_r}^{(l)}, X_{K,}^{(l)}$ equal $(N_f + K - 1)$

So, we derived the total hits between $X_{K,\tau}^{(l,l')}\ X_K^{(l,l')}$ are at most 2 $(N_f + K - 1)$

3) when τ takes other values expect those given in 1) and 2) the parameter $\tau_f \neq 0$ and

$\tau_e \neq 0$,at this time when ξ_h take an odd number $X_{K,\tau}^{(l,l')}$can be writing as $\tilde{X}_{K,\tau}^{(l,l')}$=$[\tilde{X}_{K,N_f-\lambda}^{(l)}\ \tilde{X}_{K,\lambda}^{(l')}\ \tilde{X}_{K,N_f-\lambda}^{(l)}\ \tilde{X}_{K,\lambda}^{(l')}]$ or $\tilde{X}_{K,\tau}^{(l',l)}$=$\left[\tilde{X}_{K,N_f-\lambda}^{(l')}\ \tilde{X}_{K,\lambda}^{(l)}\ \tilde{X}_{K,N_f-\lambda}^{(l')}\ \tilde{X}_{K,\lambda}^{(l)}\right]$when ξ_h

Takes an even number: $\lambda = (\tau_f - \xi_h N_f^2)/N_f$, is the TH frame shift number $0 < \lambda < N_f$

The relationship between $X_{K,\tau}^{(l,l')}$ and $\tilde{X}_{K,\tau}^{(l,l')}$ is shown as fig. in which the matrices:

$\tilde{X}_{K,\lambda}^{(l)} = \left[\tilde{x}_{\xi_r,\tau_e,0}^{(l)}\ \ \tilde{x}_{\xi_r,\tau_e,1}^{(l)}\ \ \ \tilde{x}_{\xi_r,\tau_e,\lambda-1}^{(l)}\right]$ and $\tilde{X}_{K,N_f-\lambda}^{(l)} = \left[\tilde{\mathrm{x}}_{\xi_r,\tau_e,\lambda}^{(l)}\ \ \tilde{\mathrm{x}}_{\xi_r,\tau_e,\lambda+1}^{(l)}\ \ \ \tilde{\mathrm{x}}_{\xi_r,\tau_e,N_f-1}^{(l)}\right]$

Where $\tilde{\mathrm{x}}_{\xi_r,\tau_e,\lambda}^{(l)} = [x_{i_{\xi_r},m}^{(l)} \oplus \tau_e\ ,\ x_{i_{\xi_r\oplus 1},m}^{(l)} \oplus \tau_e\ ,\ x_{i_{\xi_r\oplus(K-1)},m}^{(l)} \oplus \tau_e\ ]\ m = 0,1,\ldots N_f - 1$

Because the maximum number of hits between $X_K^{(l,l')}$ and $\tilde{X}_{K,\tau}^{(l',l)}$ is the same as that between $\tilde{X}_{K,\tau}^{(l,l')}$ and $X_K^{(l,l')}$ tilde, only the latter case is considered. Then, from Fig. 3, it is evident that the hits between $X_K^{(l,l')}$and $\tilde{X}_{K,\tau}^{(l,l')}$ consist of the following:

- partial self-hits between $X_K^{(l)}$and $\tilde{X}_{K,N_f-\lambda}^{(l)}$
- partial cross-hits between $X_K^{(l)}$ and $\tilde{X}_{K,\lambda}^{(l')}$
- partial self-hits between $X_K^{(l')}$and $\tilde{X}_{K,N_f-\lambda}^{(l')}$
- partial cross-hits between $X_K^{(l')}$and $\tilde{X}_{K,\lambda}^{(l)}$

o obtain the partial self-hits in case (a), we select the first $N_f-\lambda$ columns of $X_K^{(l)}$ to correlate with $\tilde{X}_{K,N_f-\lambda}^{(l)}$ Since they originate from the same THSI base matrix, according to Theorem 1, the maximum total partial self-hit count between $X_K^{(l)}$and $\tilde{X}_{K,N_f-\lambda}^{(l)}$is $N_f-\lambda$ This observation also holds true for the partial self-hits in case (c).

To obtain the partial cross-hits in case (b),we select two different rows denoted by $V_{i_\alpha}^{(l,l')}=\left[V_{i_\alpha}^{(l)}\ V_{i_\alpha}^{(l')}\right]$and $V_{i_\beta}^{(l,l')}=\left[V_{i_\beta}^{(l)}\ V_{i_\beta}^{(l')}\right]$ from$X_K^{(l,l')}$ and two different shifted results denoted by $\tilde{V}_{i_{\alpha'},\lambda}^{(l,l')}=\left[\tilde{V}_{i_{\alpha',N_f-\lambda}}^{(l)}\ \tilde{V}_{i_{\alpha',\lambda}}^{(l')}\ \tilde{V}_{i_{\alpha',N_f-\lambda}}^{(l')}\ \tilde{V}_{i_{\alpha'\oplus1,\lambda}}^{(l)}\right]$ and $\tilde{V}_{i_{\beta',\lambda}}^{(l,l')}=\left[\tilde{V}_{i_{\beta',N_f-\lambda}}^{(l)}\ \tilde{V}_{i_{\beta',\lambda}}^{(l')}\ \tilde{V}_{i_{\beta',N_f-\lambda}}^{(l')}\ \tilde{V}_{i_{\beta'\oplus1,\lambda}}^{(l)}\right]$from as shown in Fig.3(a) and (b),respectively.

Here, α,β,α' and β' are selected from the set$\{0,1,\ldots,K-1\}$,and $\alpha'\neq\beta'$, $\alpha=\alpha'\oplus\xi_r$and $\beta=\beta'\oplus\xi_r$where $\xi_r$is the given shift.

According to Theorem 2,when$V_{i_\alpha}^{(l)}$ of $V_{i_\alpha}^{(l,l')}$ and $\tilde{V}_{i_{\alpha'}}^{(l')}$ of $\tilde{V}_{i_{\alpha',\lambda}}^{(l,l')}$ meet the condition $i_\alpha\oplus l'=i_{\alpha'}\oplus l$,they may cause λ hits.

Similarly, for the other rows of $X_K^{(l)}$ and $\tilde{X}_{K,\lambda}^{(l')}$,they may cause $K-1$ hits at most.

Thus, the total cross-hit count between $X_K^{(l)}$and $\tilde{X}_{K,\lambda}^{(l')}$ is at most $N_f+\lambda-1$.

This observation also holds true for the partial cross-hits in case (d) when the condition $i_\beta\oplus l=i_{\beta'\oplus1}\otimes l'$ is met.

With the results from cases (a) to (d) the total hits between $X_K^{(l,l')}$ and $\tilde{X}_{K,\tau}^{(l',l)}$ under case (3) can be determined as $2(N_f + K - 1)$ at most.

Finally ,based on these results and $R_{\vartheta(l,l')}(0) = 2KN_f$ the upper bound of the subpeak of $R_{\vartheta(l,l')}(\tau)$(normalized to $R_{\vartheta(l,l')}(0)$ can be easily calculated to be $(N_f + 2K - 2)/KN_f$ where $\tau \in \mathbb{Z}$ and $0 \leq \tau \leq 2KN_f^2 - 1$ and Similarly, the property of $C_{\vartheta(l,l')}(\tau)$ can also be determined.

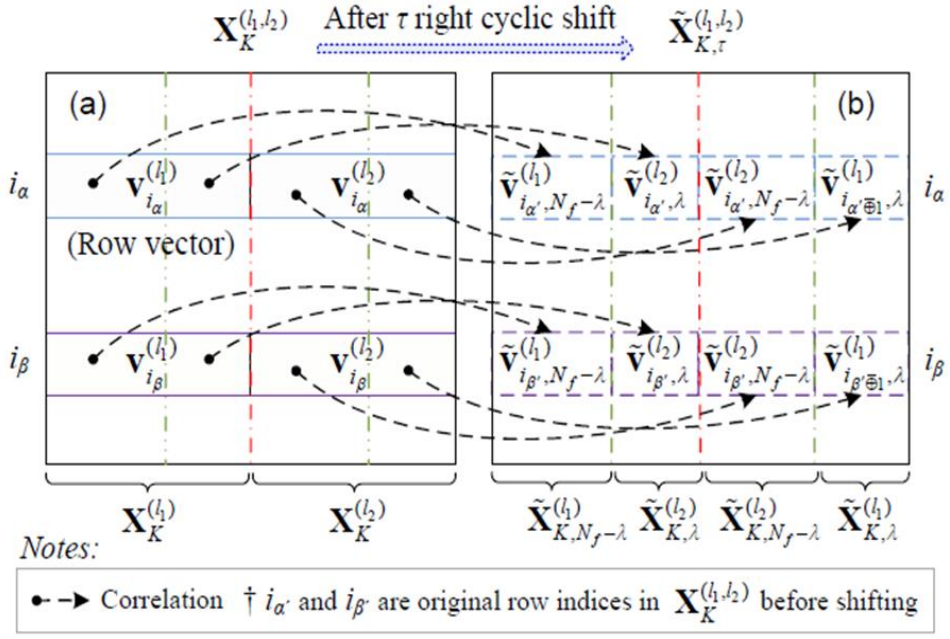

Figure 2.3 :Correlation between $X_K^{(l,l')}$and its τ cyclic shift results $\tilde{X}_{K,\tau}^{(l,l')}$ under $\tau = \tau_f + \tau_e$ where τ_f *and* $\tau_e \neq 0$[44]

2.7 SIT Detection of the Received PL Signal

In addition to creating SITs for various Payloads PLs at the transmitting end, detecting the SIT within the PL signal at the receiving end is crucial for enabling the assistance function of the PL. Typically, this involves converting the SIT detection into a search for TH pulse positions within the received PL signal, which can be achieved through three main steps: generating auto-correlation peaks of PRN codes, computing the intervals between consecutive pulses, and utilizing these intervals to determine the pulse positions of the PL signal[44].

2.7.1 Generation of the Underlying PRN Code Auto-correlation Peaks

The primary objective of generating the auto-correlation peaks of the PRN code is to determine the time intervals between consecutive TH pulses within a single TH pulse pattern. Initially, it is essential to establish the initial phase of the PRN code to ensure accurate generation of the auto-correlation peaks [47]. Despite the discontinuous nature of the received pulsed PL signal, the approach used to determine the initial phase of a continuous GNSS satellite signal can still be employed for the PL signal Based on Fig.2.1 and using the parallel PRN code phase search acquisition method, the principle of acquiring the PRN code initial phase τprn of the received PL signal can be given as [44]:

$$\tau_{prn} = \underset{\hat{\tau}_c}{arg}\left(\underset{\hat{\tau}_c, \hat{f}_{Dop}}{max}\sqrt{I^2_{\hat{C}_m}(\hat{\tau}_c, \hat{f}_{Dop}) + Q^2_{\hat{C}_m}(\hat{\tau}_c, \hat{f}_{Dop})}\right) \tag{2.9}$$

Where $\hat{\tau}_c, \hat{f}_{Dop}$ are the are the estimated PRN code initial phase, Doppler frequency $I_{\hat{C}_m}(\hat{\tau}_c, \hat{f}_{Dop})$ and $Q_{\hat{C}_m}(\hat{\tau}_c, \hat{f}_{Dop})$ are in-phase and quadrature phase integration results of two consecutive TH frames, respectively[3].

The locally generated baseband signal can be expressed as:

$$S_{\hat{C}_m}(\tau_{prn}) = \sum_{m=0}^{M-1} \hat{C}_m u_{T_{ch}}(t - mT_{ch} - \tau_{prn}) \tag{2.10}$$

where T_{ch} is the period of one PRN code chip with m is number of chips ,we select Δt time from a receiving signal and the period of integration is $N_f T_p$ so $k = \lfloor \Delta t / N_f T_p \rfloor$ is the number of period integration in Δt where $0 \leq k \leq \lfloor \Delta t / N_f T_p \rfloor - 1$,then by correlating $s_{\hat{C}_m}$ with the received signal in each interval $[kN_f T_p, (k+1)N_f T_p]$.[44]

The auto-correlation peaks of the underlying PRN code sequence and their corresponding positions can be effortlessly identified.

2.7.2 Calculation of the TH Pulse Intervals

To enhance the probability of detecting the SIT within the PL signal, a binary code sequence is derived from the intervals of the auto-correlation peaks. This binary code sequence is then utilized for detecting the SIT of the PL signal, which can improve the overall detection performance. By mapping the auto-correlation peak intervals to a binary code sequence, the detection process becomes more robust and accurate, leading to a higher probability of

successfully detecting the SIT within the PL signal. Suppose N_t auto-correlation peaks have been found and their positions are: [44]

$$\{p_k, k = 0, \dots\dots\dots N_t - 1\}$$

then the TH pulse intervals of the PL signal in unit of Tp can be calculated by:

$$\Lambda_{k-1,k} = \left\lfloor \frac{p_k - p_{k-1}}{T_p f_s} \right\rfloor, \quad k = 1, \dots\dots\dots N_t - 1 \tag{2.11}$$

where: f_s the sampling frequency.

2.7.3 Binary Mapping of the TH Pulse Intervals

From this $\Lambda_{k-1,k}$, $k = 1, \dots N_t - 1$ the mapped binary code sequence can be obtained by [44]:

$$\mathbf{H} = \left\{ h(i), i = 0, \dots\dots\dots\dots \sum_{k=1}^{N_t-1} \Lambda_{k-1,k} \right\} \tag{2.12}$$

where the element:

$$h(i) = \begin{Bmatrix} 1, i = \sum_{k=1}^{J} \Lambda_{k-1,k}, J = 0, \dots\dots\dots N_t - 1 \\ 0, \qquad\qquad\qquad\qquad other\ wise \end{Bmatrix} \tag{2.13}$$

2.7.4 Binary Mapping of the SITs in received signal

Just like the process used to derive the binary code sequence from the intervals of auto-correlation peaks, it's possible to map each SIT stored in the receiver into a binary code sequence. To clarify further, the binary code sequence derived from the ζ_th SIT of total N stored results can be given as [44]:

Where $\zeta = 1,2,3 \dots \dots N$, and the element:

$$\mathbf{B}^{(\zeta)} = \left\{ b^{(\zeta)}(i), i = 0,1, \dots\dots\dots 2KN_f - 1 \right\} \tag{2.14}$$

$$b^{(\zeta)}(i) = \begin{cases} 1, & i = a_j^{(\zeta)}, j = 0,1, \dots\dots, 2KN_f - 1 \\ 0, & otherwise \end{cases} \tag{2.15}$$

2.7.5 Pulse Position Detection of the PL Signal

Once the mapped binary code sequences of auto-correlation peak intervals and the total stored SITs are obtained, detecting the pulse positions of the transmitted PL signal involves a straightforward circular correlation operation. The detailed detection process is as follows [44]:

$$p^{(\hat{\zeta})} = \underset{i,\zeta}{arg} \left(\begin{matrix} max\, max \\ i = 0,1, \dots L-1 \\ \zeta = 0,1, \dots . N \end{matrix} \left(\overline{\mathbf{H}}(i) \otimes \widetilde{\mathbf{B}}^{(\zeta)}(i) \right) \right) \tag{2.16}$$

where $\hat{\zeta}$ represents the estimated SIT group ID used by the PL signal, and $\otimes$ denotes the circular correlation operation. $\overline{\mathbf{H}}(i)$and $\widetilde{\mathbf{B}}^{(\zeta)}(i)$ represent the code sequences of $\overline{\mathbf{H}}$ and $\widetilde{\mathbf{B}}^{(\zeta)}$after i circular shifts, respectively. Here, $\overline{\mathbf{H}}$ and $\widetilde{\mathbf{B}}^{(\zeta)}$are respectively the interpolated sequences of $\mathbf{H}$ and $\mathbf{B}^{(\zeta)}$[44].

2.8 Conclusion

In this chapter, firstly we presented the new method for detecting the positions of TH pulses Next, we give a few code sequences mapped from the SIT and the TH slit indices. Finally, we presented the detection method. in the following chapter we will discuss the simulation results and their interpretation.

Chapter 3 :

Result and Discussion

3.1 Introduction

In this chapter, we present the results of numerical simulations on the different methods of generation and detection of the pseudolite TH pulse position that we have implemented on MATLAB. Firstly, we will present this SIT with CC-based method and the RP method and the acquisition results that show the detection of the pseudo-random positions of the TH pulses of the two delays, namely the delay of the PRN code (τ_{prn}) and the delay of the TH slit indices (τ_{ip}). The results obtained are then subjected to the probability of detection criterion.

3.2 Performance of detection

3.2.1 Digital simulation parameters

To assess the effectiveness of the proposed method in generating SITs, we conduct simulations to examine the properties of the THSI distributions, correlations, and PSD of the generated SITs. Furthermore, we investigate the ability of SIT detection in the receiving end to identify the PL signal.

Table 3.1 : table of parameters

Sampling frequency	$f_s = 12MHz$
The intermediate frequency	$f_{IF} = 4.309MHz$
Doppler frequency	$f_{Dop} = 800Hz$
Duty cycle	$d = 0.1$
Total number of frame TH	$K = 10$
Number of frames	$N_f = 10$
PRN code period	$T_c = 1ms$
PL pulse duration	$T_p = 0.1ms$
data bit periods of GNSS-like Signal	$T_b = 20ms$
période of PL signal	$200ms$
The period of one TH frame	$T_c = 1ms$
the PRN code of the PL signal	$1023\ chips$
The initial phase of PRN code	$\tau_{prn} = 220\ chips$

3.2.2 Simulations on THSI Distribution of Different SITs

Just as we explained earlier that the number of THSI needed for one SIT is obtained by combining two matrices, we calculated four matrices $X^{(1)}, X^{(6)}, X^{(4)}, X^{(8)}$ for two SITs $X^{(16)} = [X^{(1)}X^{(6)}] and\ X^{(48)} = [X^{(4)}X^{(8)}]$ We concatenated to obtained a SIT And we create in others SITs with the Rand Perm method

$$X^{(1)} = \begin{bmatrix} 0 & 1 & 2 & 3 & 4 & 5 & 6 & 7 & 8 & 9 \\ 1 & 3 & 5 & 7 & 9 & 0 & 2 & 4 & 6 & 8 \\ 2 & 5 & 8 & 0 & 3 & 6 & 9 & 1 & 4 & 7 \\ 3 & 7 & 0 & 4 & 8 & 1 & 5 & 9 & 2 & 6 \\ 4 & 9 & 3 & 8 & 2 & 7 & 1 & 6 & 0 & 5 \\ 5 & 0 & 6 & 1 & 7 & 2 & 8 & 3 & 9 & 4 \\ 6 & 2 & 9 & 5 & 1 & 8 & 4 & 0 & 7 & 3 \\ 7 & 4 & 1 & 9 & 6 & 3 & 0 & 8 & 5 & 2 \\ 8 & 6 & 4 & 2 & 0 & 9 & 7 & 5 & 3 & 1 \\ 9 & 8 & 7 & 6 & 5 & 4 & 3 & 2 & 1 & 0 \end{bmatrix} \quad X^{(6)} = \begin{bmatrix} 5 & 0 & 6 & 1 & 7 & 2 & 8 & 3 & 9 & 4 \\ 0 & 1 & 2 & 3 & 4 & 5 & 6 & 7 & 8 & 9 \\ 6 & 2 & 9 & 5 & 1 & 8 & 4 & 0 & 7 & 3 \\ 1 & 3 & 5 & 7 & 9 & 0 & 2 & 4 & 6 & 8 \\ 7 & 4 & 1 & 9 & 6 & 3 & 0 & 8 & 5 & 2 \\ 2 & 5 & 8 & 0 & 3 & 6 & 9 & 1 & 4 & 7 \\ 8 & 6 & 4 & 2 & 0 & 9 & 7 & 5 & 3 & 1 \\ 3 & 7 & 0 & 4 & 8 & 1 & 5 & 9 & 2 & 6 \\ 9 & 8 & 7 & 6 & 5 & 4 & 3 & 2 & 1 & 0 \\ 4 & 9 & 3 & 8 & 2 & 7 & 1 & 6 & 0 & 5 \end{bmatrix}$$

$$X^{(16)} = \begin{bmatrix} 0 & 1 & 2 & 3 & 4 & 5 & 6 & 7 & 8 & 9 & 5 & 0 & 6 & 1 & 7 & 2 & 8 & 3 & 9 & 4 \\ 1 & 3 & 5 & 7 & 9 & 0 & 2 & 4 & 6 & 8 & 0 & 1 & 2 & 3 & 4 & 5 & 6 & 7 & 8 & 9 \\ 2 & 5 & 8 & 0 & 3 & 6 & 9 & 1 & 4 & 7 & 6 & 2 & 9 & 5 & 1 & 8 & 4 & 0 & 7 & 3 \\ 3 & 7 & 0 & 4 & 8 & 1 & 5 & 9 & 2 & 6 & 1 & 3 & 5 & 7 & 9 & 0 & 2 & 4 & 6 & 8 \\ 4 & 9 & 3 & 8 & 2 & 7 & 1 & 6 & 0 & 5 & 7 & 4 & 1 & 9 & 6 & 3 & 0 & 8 & 5 & 2 \\ 5 & 0 & 6 & 1 & 7 & 2 & 8 & 3 & 9 & 4 & 2 & 5 & 8 & 0 & 3 & 6 & 9 & 1 & 4 & 7 \\ 6 & 2 & 9 & 5 & 1 & 8 & 4 & 0 & 7 & 3 & 8 & 6 & 4 & 2 & 0 & 9 & 7 & 5 & 3 & 1 \\ 7 & 4 & 1 & 9 & 6 & 3 & 0 & 8 & 5 & 2 & 3 & 7 & 0 & 4 & 8 & 1 & 5 & 9 & 2 & 6 \\ 8 & 6 & 4 & 2 & 0 & 9 & 7 & 5 & 3 & 1 & 9 & 8 & 7 & 6 & 5 & 4 & 3 & 2 & 1 & 0 \\ 9 & 8 & 7 & 6 & 5 & 4 & 3 & 2 & 1 & 0 & 4 & 9 & 3 & 8 & 2 & 7 & 1 & 6 & 0 & 5 \end{bmatrix}$$

$$X^{(4)} = \begin{bmatrix} 3 & 7 & 0 & 4 & 8 & 1 & 5 & 9 & 2 & 6 \\ 7 & 4 & 1 & 9 & 6 & 3 & 0 & 8 & 5 & 2 \\ 0 & 1 & 2 & 3 & 4 & 5 & 6 & 7 & 8 & 9 \\ 4 & 9 & 3 & 8 & 2 & 7 & 1 & 6 & 0 & 5 \\ 8 & 6 & 4 & 2 & 0 & 9 & 7 & 5 & 3 & 1 \\ 1 & 3 & 5 & 7 & 9 & 0 & 2 & 4 & 6 & 8 \\ 5 & 0 & 6 & 1 & 7 & 2 & 8 & 3 & 9 & 4 \\ 9 & 8 & 7 & 6 & 5 & 4 & 3 & 2 & 1 & 0 \\ 2 & 5 & 8 & 0 & 3 & 6 & 9 & 1 & 4 & 7 \\ 6 & 2 & 9 & 5 & 1 & 8 & 4 & 0 & 7 & 3 \end{bmatrix} \quad X^{(8)} = \begin{bmatrix} 7 & 4 & 1 & 9 & 6 & 3 & 0 & 8 & 5 & 2 \\ 4 & 9 & 3 & 8 & 2 & 7 & 1 & 6 & 0 & 5 \\ 1 & 3 & 5 & 7 & 9 & 0 & 2 & 4 & 6 & 8 \\ 9 & 8 & 7 & 6 & 5 & 4 & 3 & 2 & 1 & 0 \\ 6 & 2 & 9 & 5 & 1 & 8 & 4 & 0 & 7 & 3 \\ 3 & 7 & 0 & 4 & 8 & 1 & 5 & 9 & 2 & 6 \\ 0 & 1 & 2 & 3 & 4 & 5 & 6 & 7 & 8 & 9 \\ 8 & 6 & 4 & 2 & 0 & 9 & 7 & 5 & 3 & 1 \\ 5 & 0 & 6 & 1 & 7 & 2 & 8 & 3 & 9 & 4 \\ 2 & 5 & 8 & 0 & 3 & 6 & 9 & 1 & 4 & 7 \end{bmatrix}$$

$$X^{(48)} = \begin{bmatrix} 3 & 7 & 0 & 4 & 8 & 1 & 5 & 9 & 2 & 6 & 7 & 4 & 1 & 9 & 6 & 3 & 0 & 8 & 5 & 2 \\ 7 & 4 & 1 & 9 & 6 & 3 & 0 & 8 & 5 & 2 & 4 & 9 & 3 & 8 & 2 & 7 & 1 & 6 & 0 & 5 \\ 0 & 1 & 2 & 3 & 4 & 5 & 6 & 7 & 8 & 9 & 1 & 3 & 5 & 7 & 9 & 0 & 2 & 4 & 6 & 8 \\ 4 & 9 & 3 & 8 & 2 & 7 & 1 & 6 & 0 & 5 & 9 & 8 & 7 & 6 & 5 & 4 & 3 & 2 & 1 & 0 \\ 8 & 6 & 4 & 2 & 0 & 9 & 7 & 5 & 3 & 1 & 6 & 2 & 9 & 5 & 1 & 8 & 4 & 0 & 7 & 3 \\ 1 & 3 & 5 & 7 & 9 & 0 & 2 & 4 & 6 & 8 & 3 & 7 & 0 & 4 & 8 & 1 & 5 & 9 & 2 & 6 \\ 5 & 0 & 6 & 1 & 7 & 2 & 8 & 3 & 9 & 4 & 0 & 1 & 2 & 3 & 4 & 5 & 6 & 7 & 8 & 9 \\ 9 & 8 & 7 & 6 & 5 & 4 & 3 & 2 & 1 & 0 & 8 & 6 & 4 & 2 & 0 & 9 & 7 & 5 & 3 & 1 \\ 2 & 5 & 8 & 0 & 3 & 6 & 9 & 1 & 4 & 7 & 5 & 0 & 6 & 1 & 7 & 2 & 8 & 3 & 9 & 4 \\ 6 & 2 & 9 & 5 & 1 & 8 & 4 & 0 & 7 & 3 & 2 & 5 & 8 & 0 & 3 & 6 & 9 & 1 & 4 & 7 \end{bmatrix}$$

The rand-perm is a function in MATLAB generates a random permutation of integers from 1 to n because it gives values like those in the Locata schemes and we compared them the RP method and proposed method of distributing THSI interval in figure 3.2 and 3.3.

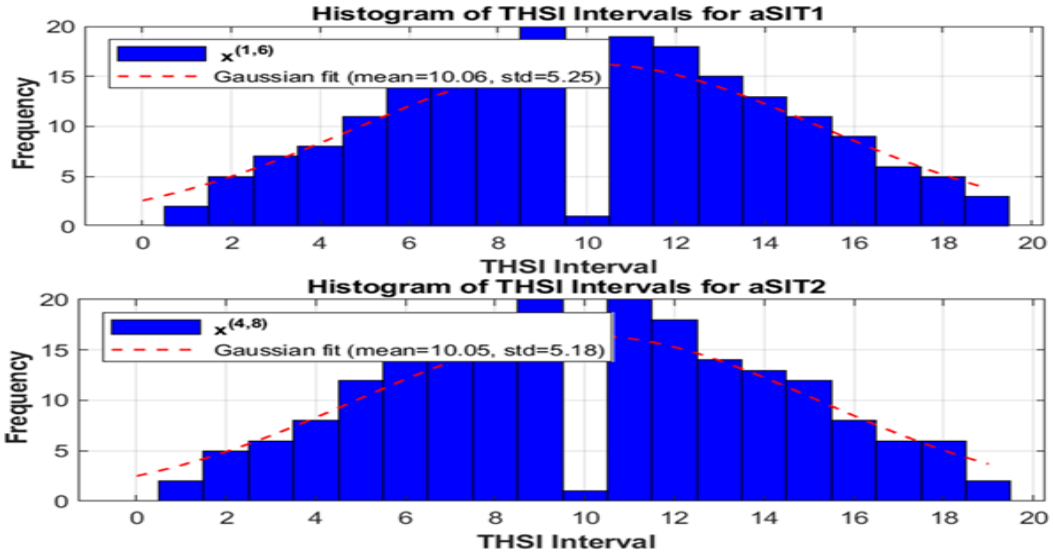

Figure 3.1 ; Histograms of different SIT given by CC-based method

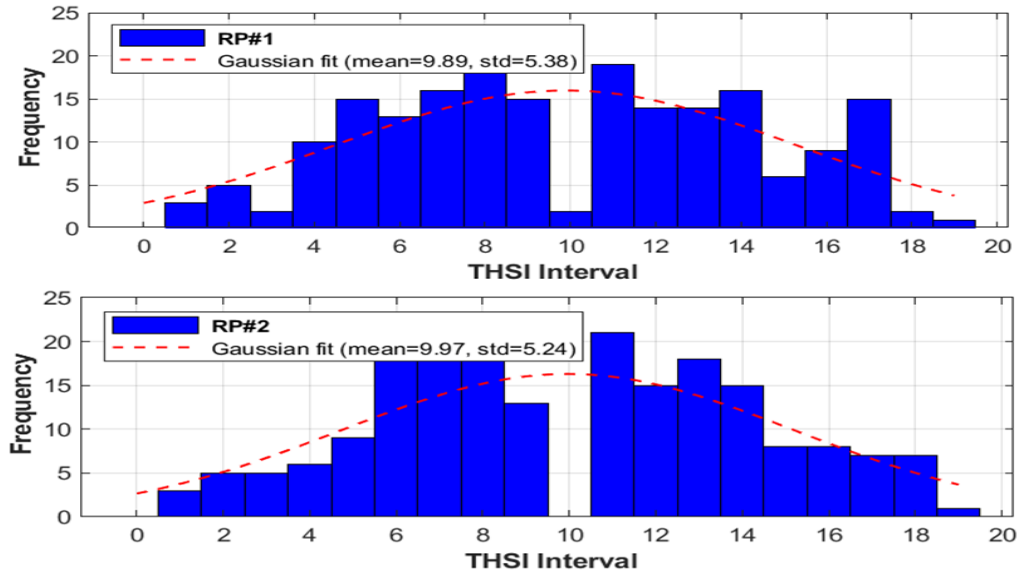

Figure 3.2 ; Histograms of different SIT given by RP Method

From Figures 3.1 and 3.2, we observe that:

The average THSI period of the CC-based method is closely aligned with the average THSI period, but it shows a more significant variation in standard error than the latter. This variation can help detect the transmitted PL signal. For the CC-based method THSI intervals with a frequency of 10 are lower than in the RP method. This reduction can minimize the likelihood of generating false spectral lines while tracking the PL signal

However, it should be noted that the RP method offers the advantage that the frequency of THSI breaks equal to 1 is equal to zero. This feature helps to avoid detection ambiguity associated with two neighbouring binary THSI intervals.

3.2.3 Simulations on Correlation Properties of the Formed SITs

The correlation characteristic of the modulated SIT directly affects the detection performance of the generated PL signal.

To verify the correlation performance of the the CC-based method, simulations were conducted on the ACF and CCF characteristics of different SITs provided by the the CC-based method and the RP method, and the results are shown.

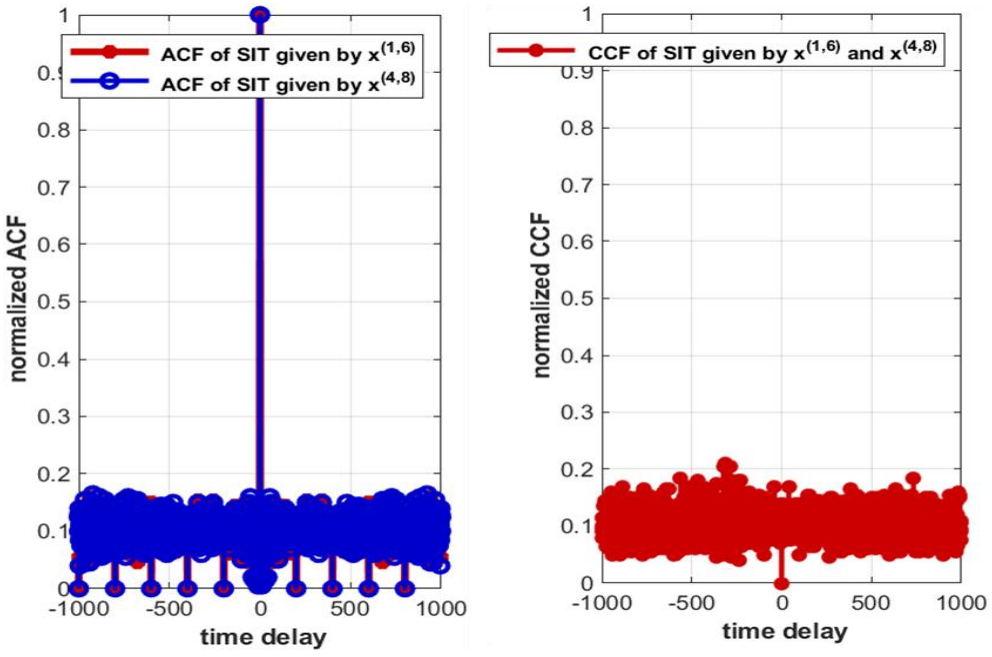

Figure 3.3 ; ACF and CCF of deferent SITs given by CC-based method

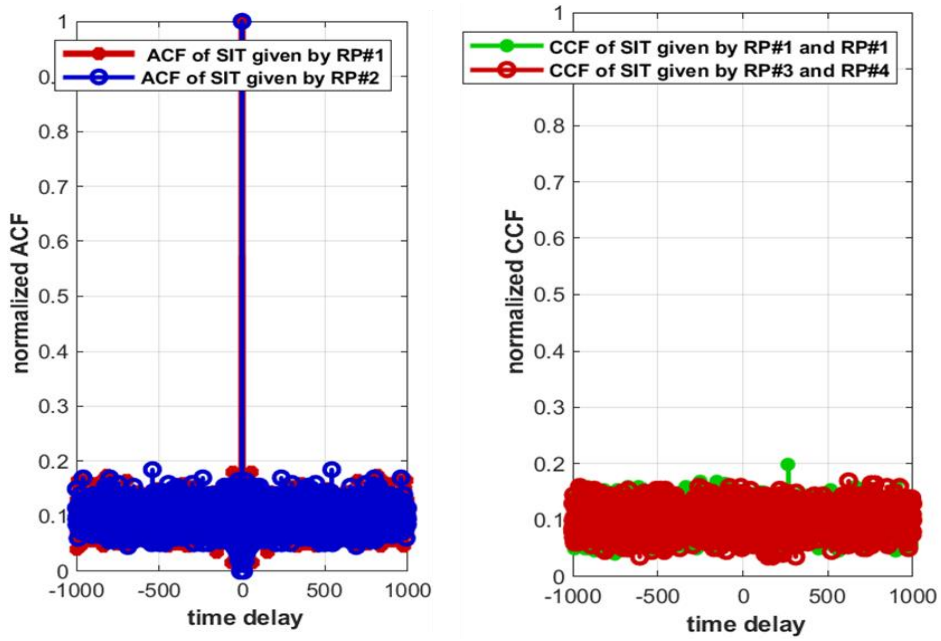

Figure 3.4 ; ACF and CCF of different SITs given by RP Method

From Figures 3.3 and 3.4 it is easily seen that the ACF performance of the the CC-based method is better than that of the RP methods, and the CCF performance of CC-based method is comparable to that of the RP methods. More specifically, from the comparison, it can be easily seen that the maximum sub-peak frequencies of ACF of the proposed method in Fig. 3.3 are lower than that of the RP methods in Fig.3.4 Here, the ACF sub-peak upper bound and CCF peak upper bound can be calculated the upper peak limit can be calculated as 0.19 (-14.42 dB) and 0.28 (-11.06 dB) by Theorem 3 and Corollary 1, respectively.

To summarize, if the performance of both ACF and CCF are considered, the CC-based method is relatively better than the RP methods.

3.2.4 Simulations on PSD of the Formed SITs

Simulations were conducted to analyse the PSD characteristics of the SITs generated by the CC based method alongside RP methods to assess the SIT formation's effectiveness comprehensively. By examining the PSD profiles of the different SITs, insights into their frequency domain properties were gained, providing a deeper understanding of their spectral distributions and energy concentrations across various frequency bands. This analysis validates the proposed method's efficacy in generating SITs with desirable PSD attributes compared to conventional RP methods, contributing to the overall evaluation of its performance in signal processing and communication.

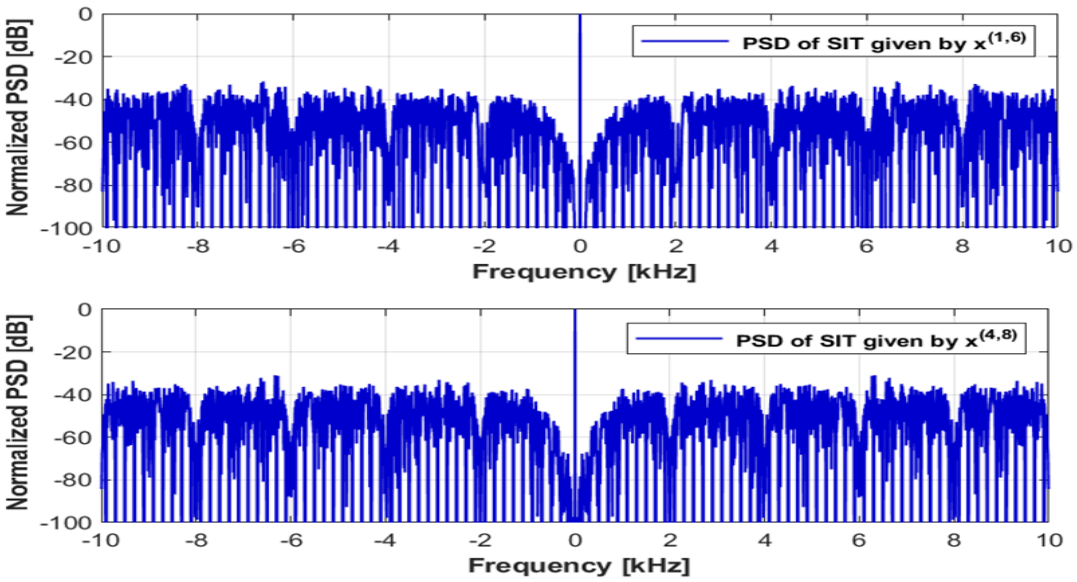

Figure 3.5 ; PSD of deferent SITs given by the CC-based method

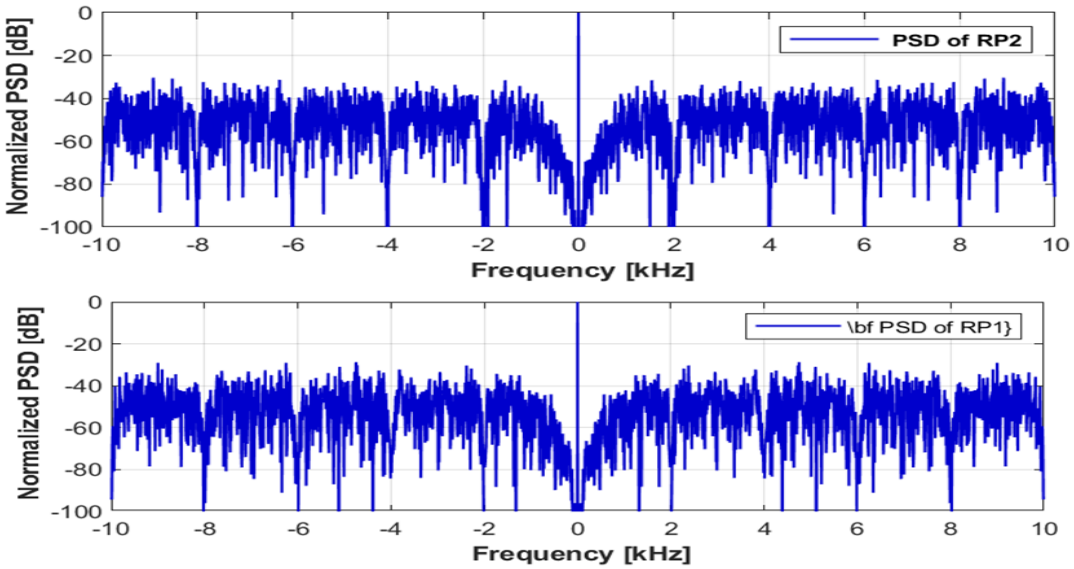

Figure 3.6 ; PSD of different SIT given by RP Method

From Figures 3.5 to 3.6, it is easily seen that the performance of PSD performance of the the CC-based method is also better than the RP method. More specifically, the sub-peak attenuation of the PSD sub-peak of the the CC-based method in Figure 9 is higher than that of the RP method, and the parameter comparisons on the average sub-peak attenuation of the CC-based method can also be exemplified. For example, the parameter for the average sub-peak attenuation of the average attenuation SITs presented by the CC-based method is about 34 dB. In contrast, for the SITs given by the RP method, this value is about 26 dB, which means that the CC-based method outperforms the RP method by about 8 dB or an improvement of about 31%. This PSD performance of the CC-based method lays a good foundation for detecting and tracking the transmitted PL signal at the receiver.

proposed is about 34 dB, while for the SITs given by the RP method, this value is about 26 dB, which means that the CC-based method outperforms the RP method by about 8 dB, or an improvement of about 31%. This PSD performance of the proposed method lays a good foundation for detecting and tracking the transmitted PL signal at the receiver.

3.2.5 Simulations on SIT Detection of the received PL Signal

To evaluate SIT detection performance of the received Positioning Signal PL signal, we follow the methodology outlined in chapter 2. This involves simulating the detection probability of the TH pulse initial phase of tow part integral part τ_{ip} and fractional part τ_{fp} for different SITs generated by both the CC-based method and RP methods. The simulation results are presented in Figures 3.7 and 3.8.

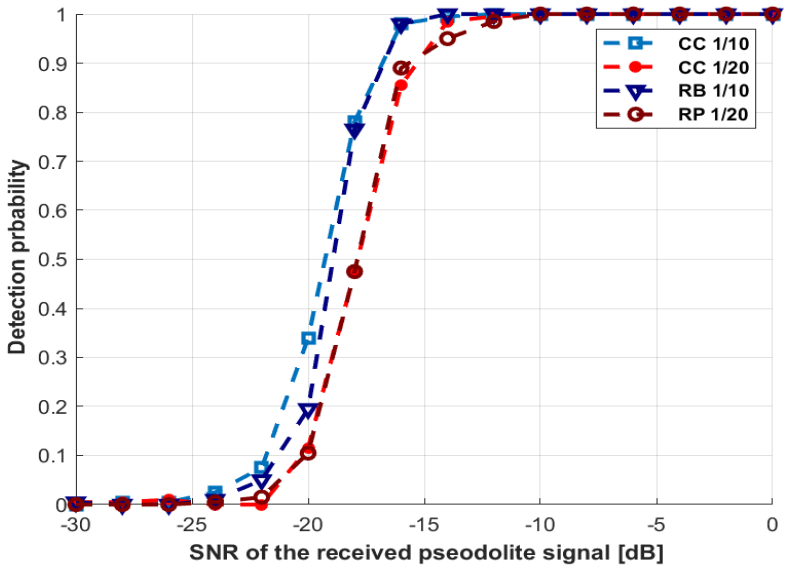

Figure 3.7 ; TH pulse initial phase detection probability of deferent given by CC-based method and RP Method

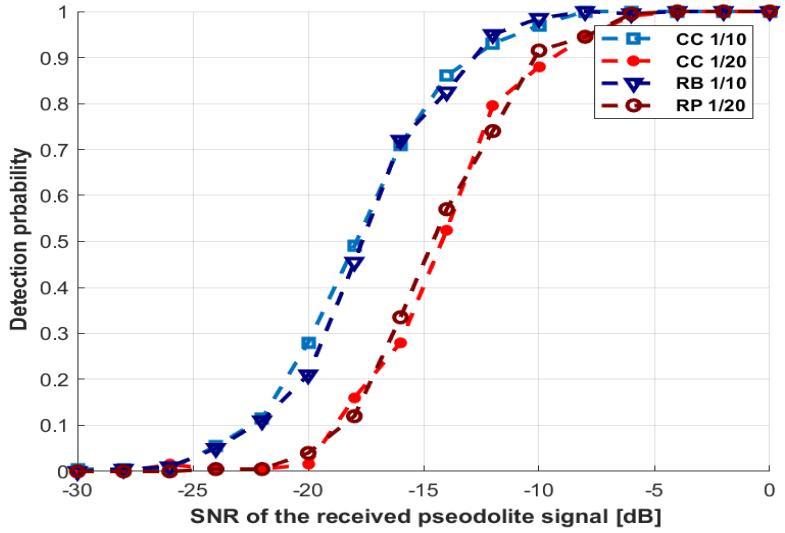

Figure 3.8 ; TH pulse initial phase detection probability of deferent given by CC-based method and RP Method

3.2.5.1 Detection Probability of Integral part

By looking at the figure, we can see the effectiveness of this CC-based method, that under the same d and SNR, TH initial phase detection probability of the SIT given by the CC-based method outperforms that of the SIT given by the RP method. For example, under d = 1/10 and SNR = -20 dB, the detection probability of the CC-based method is about 0.35, and this result will fall to 0.15for the RP method and between -15 and -5dB, the detection probability of the CC-based method and RP it's the same and when d = 1/20 the detection probability of the CC-based method and RP method it's the same almost.

3.2.5.2 Detection Probability of Fractional part

By looking at the figure, we can see the effectiveness of this CC-based method, that under the same d and SNR, TH initial phase detection probability of the SIT given by the CC-based method outperforms that of the SIT given by the RP method. For example, under d = 1/10 and SNR = -20 dB, the detection probability of the CC-based method is about 0.28, and this result will fall to 0.1for the RP method and between -15: -5dB, the detection probability of the CC-based method and RP it's the same when d = 1/20 the detection probability of the CC-based method and RP method it's the same almost.

3.3 Conclusion

In this chapter, we have presented the numerical simulation results for the different methods we have implemented for generating the TH pseudolite pulse position., the simulation results for the validation of this technique were presented and discussed. Finally, a comparative study of the performance results, based on the probability of error criterion, was carried out.

General Conclusion

General Conclusion

A recent method for generating the pseudorandom positions of TH pulses in pseudolite signals for participatory GNSS receivers has been introduced in the literature. This Master's thesis investigates this newly CC-based method for generating the pseudorandom positions of TH pulses.

First, we outlined the fundamental principles of GNSS signal generation, providing an overview of the GPS and Pseudolite systems. We then delved into the specifics of the CC-based method for generating the pseudorandom positions of TH pulses. To validate this method, we performed MATLAB simulations, demonstrating its practical application and effectiveness.

The performance of this CC-based method was rigorously tested using the correlation property and TH pulse detection probability,. Our findings revealed that compared to other similar schemes the CC-based method offers superior performance. This indicates its potential for enhancing the robustness and reliability of pseudolite signals in challenging conditions.

We propose to validate other methods for generating pseudo-random positions for TH pulses and to carry out a comparative study to classify these generation methods.

Bibliography

Bibliography

*[1] C. O'Driscoll, D. Borio, and J. Fortuny-Guasch, "Investigation of pulsing schemes for pseudolite applications," in *Proceedings of the 24th International Technical Meeting of the Satellite Division of The Institute of Navigation (ION GNSS 2011)*, pp. 3480-3492, Sep. 2011.*

*[2] D. Borio and C. O'Driscoll, "Design of a general pseudolite pulsing scheme," *IEEE Transactions on Aerospace and Electronic Systems*, vol. 50, no. 1, pp. 2-16, 2014.*

*[3] Y. Hu, B. Yu, M. Song, and Z. Deng, "Pulse Position Detection of the Pseudo Random Time-Hopping Pseudolite for the Participative GNSS Receivers," *IEEE Access*, vol. 8, pp. 216151-216161, 2020.*

[4] J. W. Cheong, "Signal processing and collective detection for Locata positioning system," Ph.D. dissertation, UNSW Sydney, 2012.

*[5] L. Tao, J. Sun, G. Li, and B. Zhu, "An improved navigation pseudolite signal structure based on the Kasami sequences and the pulsing scheme," *Chinese Journal of Electronics*, vol. 31, no. 2, pp. 220-226, 2022.*

[6] E. D. Kaplan and C. J. Hegarty, Understanding GPS: Principles and Applications, 2nd ed. Artech House, 2006.

[7] W. H. Wooden, "Navstar Global Positioning System," in Proceedings of the first International Symposium on Precise Positioning with Global Positioning System, vol. 1, pp. 23-32, 15-19 April 1985.

[8] ICD-GPS-200C, "Interface Control Document Navstar GPS Space Segment/Navigation," User Interfaces. US DOD, IRN-200C-005R1, 14 January 2003.

[9] Gps.gov, "Official U.S. government information about the Global Positioning System (GPS) and related topics," [Online]. Available: http://www.gps.gov/systems/gps/space/. [Accessed: August 2017].

[10] B. H. Wellenhof, H. Lichtenegger, and E. Wasle, GNSS – Global Navigation Satellite Systems GPS, GLONASS, Galileo, and more. Springer Wien New York, 2008.

*[11] C. Cummins, R. Orr, H. O'Connor, and C. West, "Global positioning systems (GPS) and microtechnology sensors in team sports: a systematic review," *Sports medicine*, vol. 43, pp. 1025-1042, 2013.*

*[12] P. Larsson, "Global positioning system and sport-specific testing," *Sports medicine*, vol. 33, no. 15, pp. 1093-1101, 2003.*

*[13] Y. V. E. S. Schutz and R. E. N. É. Herren, "Assessment of speed of human locomotion using a differential satellite global positioning system," *Medicine and science in sports and exercise*, vol. 32, no. 3, pp. 642-646, 2000.*

*[14] A. J. Gray, D. Jenkins, M. H. Andrews, D. R. Taaffe, and M. L. Glover, "Validity and reliability of GPS for measuring distance travelled in field-based team sports," *Journal of sports sciences*, vol. 28, no. 12, pp. 1319-1325, 2010.*

*[15] M. S. Braasch and A. J. Van Dierendonck, "GPS receiver architectures and measurements," *Proceedings of the IEEE*, vol. 87, no. 1, pp. 48-64, 1999.*

[16] ICD L1, L2 GLONASS, "Global Navigation Satellite System GLONASS," INTERFACE CONTROL DOCUMENT, Russian Space Systems, 2008.

[17] G. Beutler, A. W. Moore, and I. I. Mueller, "The international global navigation satellite systems service (IGS): development and achievements," Journal of Geodesy, vol. 83, pp. 297-307, 2009.

[18] J. Wang, "Pseudolite applications in positioning and navigation: Progress and problems," Positioning, vol. 1, no. 03, 2002.

[19] "Global Positioning System (GPS)," Encyclopædia Britannica. [Online]. Available: https://www.britannica.com/technology/GPS. [Accessed: May 3, 2024].

[20] "French SBAS - System Overview," GPS.gov. [Online]. Available: https://www.gps.gov/systems/augmentations/french.php. [Accessed: May 3, 2024].

[21] "GPS Satellite Constellation," GPS.gov. [Online]. Available: https://www.gps.gov/systems/gps/space/. [Accessed: May 3, 2024].

[22] B. Hofmann-Wellenhof, H. Lichtenegger, and J. Collins, Global Positioning System: Theory and Practice, 5th ed. New York: Springer Verlag Wien, 2001.

[23] P. K. Enge, "GPS Modernization: Capabilities of the New Civil Signals," Invited Paper for the Australian International Aerospace Congress Brisbane, 2003.

[24] S. Moad, "Conception d'un systéme de positionnement par SMS," Ph.D. dissertation.

[25] J. M. Piéplu, GPS et Galileo Systèmes de navigation par satellites. Paris: EYROLLES, 2006.

[26] J. L. Cosandier, "Global Positioning System: Principes généraux de la localisation par satellites," cours, April 2003.

[27] A. El-Rabbany, Introduction to GPS the Global Positioning System. Boston, London: ArtechHouse Mobile Communications Series, 2002.

[28] E. D. Kaplan and C. J. Hegarty, Understanding GPS: Principles and Applications, 2nd ed. Artech House, 2006

[29] J. M. Piéplu, GPS et Galileo: Systèmes de navigation par satellites. Paris: EYROLLES, 2006.

[30] J. B.Y. Tsui, Fundamentals of GPS Receivers: A software approach, 2nd ed. Wiley: John Wiley & Sons, 2002.

[31] B. Parkinson, J. Spilker, P. Axelrad, and P. Enge, "Global Positioning System: Theory and Applications."

[32] Z. Weihua and J. Tranquilla, "Modeling and Analysis For The GPS Pseudo-Range Observable," IEEE Transactions on Aerospace and Electronic Systems, vol. 31, pp. 739-751, April 1995.

[33] D. Borio, "A Statistical Theory for GNSS Signal Acquisition," Ph.D. dissertation, March 2008.

[34] W. Z. Zhuang and J. Tranquilla, "Digital Baseband Processor For The GPS Receiver (part I and II)," IEEE Transactions on Aerospace and Electronic Systems, vol. 29, no. 14, pp. 1343–1349, 1993.

[35] V. N. DJR and C. AJRM, "New Fast GPS Code-Acquisition Technique Using FFT," Electronic Lettre, vol. 27, no. 12, pp. 158–160, 1991.

[36] P. Sagiraju, G. Raju, and D. Akopian, "Fast Acquisition Implementation For High Sensitivity Global Positioning Systems Receivers Based On Joint And Reduced Space Search," IEE Proceedings on Radar, Sonar, and Navigation, vol. 2, no. 15, pp. 376-387, 2008.

[37] D. Manandhar, Y. Suh, and R. Shibasaki, "GPS signal acquisition and tracking-An Approach towards development of Software-based GPS Receiver," Technical Report of IEICE, 2004.

*[38] J. B. Y. Tsui, *Fundamentals of Global Positioning System Receivers-A Software Approach, A John Wiley & Sons. Inc. Publication*, 2nd ed., 2000.*

[39] N. Viandier, "Modélisation et utilisation des erreurs de pseudodistances GNSS en environnement transport pour l'amélioration des performances de localisation," Ph.D. dissertation, Ecole centrale de Lille, 2011.

*[40] T. A. Stansell Jr, "RTCM SC-104 recommended pseudolite signal specification," *Navigation*, vol. 33, no. 1, pp. 42-59, 1986.*

*[41] X. Feng, H. C. Wu, Y. Wu, and X. Wang, "Kasami sequence studies for DTV transmitter identification," *IEEE Transactions on Consumer Electronics*, vol. 58, no. 4, pp. 1138-1146, 2012.*

[42] H. S. Cobb, "GPS pseudolites: Theory, design, and applications," Stanford University, 1997.

*[43] P. H. Madhani, P. Axelrad, K. Krumvieda, and J. Thomas, "Application of successive interference cancellation to the GPS pseudolite near-far problem," *IEEE Transactions on Aerospace and Electronic Systems*, vol. 39, no. 2, pp. 481-488, 2003.*

*[44] Y. Hu, B. Yu, Z. Deng, and W. Yu, "Generation of Slot Index Tables for Time-Hopping Pseudolites with the Constructed Congruence Codes," *Radioengineering*, vol. 32, no. 1, pp. 113-123, 2023.*

[45]]Yang, G. C., & Kwong, W. C., "Prime codes with applications to CDMA optical and wireless networks," Artech House.

*[46] S. V. Maric and E. L. Titlebaum, "A class of frequency hop codes with nearly ideal characteristics for use in multiple-access spread-spectrum communications and radar and sonar systems," *IEEE Transactions on Communications*, vol. 40, no. 9, pp. 1442-1447, 1992.*

*[47] Z. Kostic and E. L. Titlebaum, "The design and performance analysis for several new classes of codes for optical synchronous CDMA and for arbitrary-medium time-hopping synchronous CDMA communication systems," *IEEE Transactions on Communications*, vol. 42, no. 8, pp. 2608-2617, 1994.*